Statistical shape and image analysis

Multivariate splines in automatic identification and statistical analysis of anatomical curves and surface patches

Stanislav Katina[1,2]

[1]Institute of Mathematis and Statistics, Masaryk University, Brno, CR
[2]*Honorary Research Fellow*, School of Mathematics and Statistics
University of Glasgow, Glasgow, Scotland, UK

Supported by wellcometrust

Robust
Jetřichovice, Jan 23 2014

Statistics:
Prof. Adrian Bowman, The University of Glasgow, Scotland, UK
Doc. Stanislav Katina, Masaryk University, Brno, CZ
Computer Vision:
Dr. J. Paul Siebert, The University of Glasgow, Scotland, UK
Prof. Paul F. Whelan, Dublin City University, Ireland
Dr. Federico Sukno, Dublin City University, Ireland
Mathematics and Geometry:
Dr. Kevin Hayes, The University of Limerick, Ireland
Dr. Brendan Guilfoyle, Institute of Technology, Tralee, Ireland
Medicine:
Prof. Ashraf Ayoub, The University of Glasgow, Scotland, UK
Dr. Balvinder Khambay, The University of Glasgow, Scotland, UK
Prof. John Waddington, Royal College of Surgeons in Ireland, Dublin, Ireland

1. distances vs. **(semi)landmarks on curves and surfaces**
2. **2D shapes** vs **3D/4D shapes**
3. **static** vs **animated**
4. boring vs **interesting**
5. abstract vs **real**
6. wrong vs **good direction of model choice**
7. partial (local) vs **complex (global) knowledge**
8. **biology/medicine** vs **statistics/mathematics**
9. one scientific field vs **interdisciplinary science**

Presentation Outline
Summary of Contrasts

What I would like to present you?

Research ideas through examples calculated in R, originated in my teaching and research experience, all in interesting, animated, and complex interdisciplinary form, using examples from **2D**, **3D**, or **4D shape and image analysis**, fusing five scientific fields

1. Mathematics
2. Euclidean and Differential Geometry
3. Statistics
4. Computer Vision
5. Image Processing
6. Biology, and Medicine

Shape Analysis—Interdisciplinary View

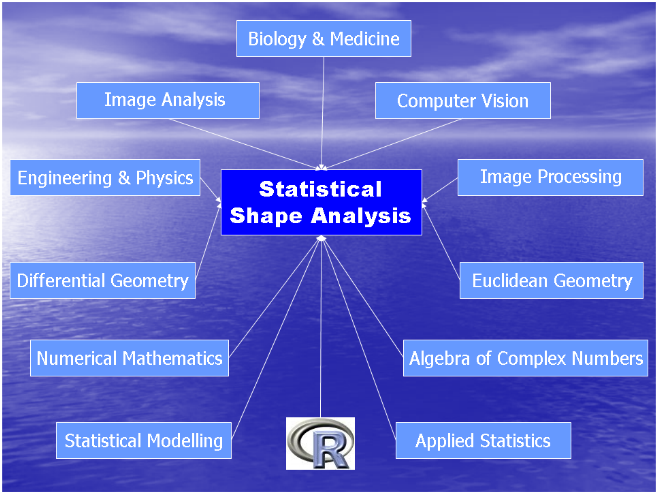

Shape Analysis Vision ≈ My Partial Research Tree

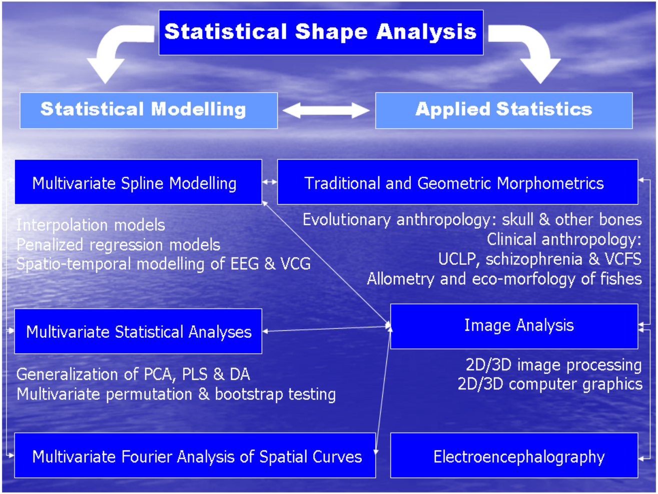

Traditional Morphometrics
Anthropological Measurement Devices

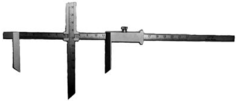

Rudolf Martin's classification

- classic system – nearly a century ago
- mainly list of endpoints for conventional distance or angle measurements
- planes and lines
- standardized views (frontalis, lateralis, verticalis, basilaris, occipitalis, sagittalis)
- lengths, widths, heights
- circumferences and surface arc length
- angles
- volumes and weights
- radii (distances of points to curves)
- indices (ratios)

Rudolf Martin's classification

- a great diversity of points (landmarks) in one or more of those standardized views
- total number of different points – 68 [Figs 286–292]
- nowadays – 158 (including some synonyms)

GM vs KM
Norma frontalis

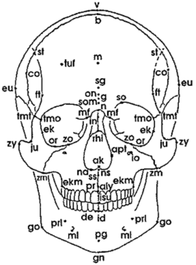

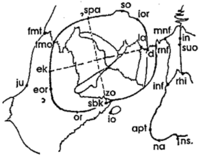

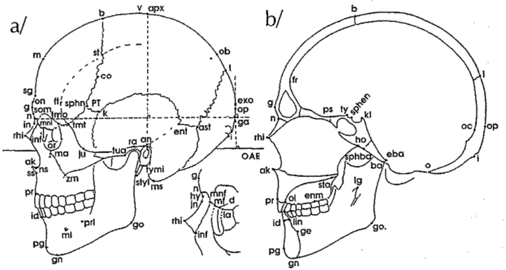
a/
b/
OAE

- neurocrania–**roaches** *Rutilus rutilus* and *Rutilus virgo* (*Actinopterygii: Cyprinidae*)
- *R. rutilus* ($n_{rr} = 30$) and *R. pigus* neurocrania ($n_{rp} = 50$), 27 measurements

Traditional vs Geometric Morphometrics

Fish Neurocrania—*Rutilus rutilus* and *R.pigus* (Cyprinidae)

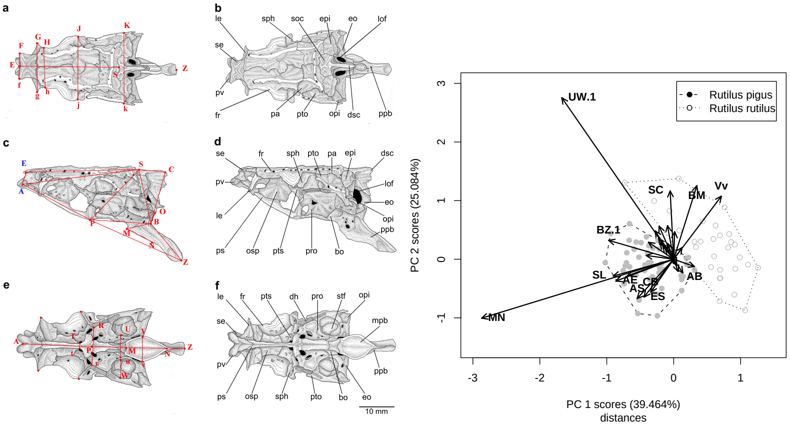

Figure: Triangulated distances and PCA of inter-landmark distances

1. **form**—information about object geometry that remains after translation and rotation effects are removed
2. **shape**—information about object geometry that remains after translation, rotation, and size effects are removed
3. **object geometry**—2D/3D Cartesian coordinates in $k \times d$ configuration matrix $\mathbf{X}$
4. **shape components**—***affine*** (uniform) $\mathbf{X}_A$, ***non-affine*** (nonuniform) $\mathbf{X}_{NA}$ [***local bending*** and ***global bending***]
5. **biological homology**—biologically correspondent parts of an organism but point locations with respect to deformation TPS model—**landmarks**
6. **geometrical homology**—with respect to some minimization criteria (***bending energy of TPS model***) between source and target configuration— **semilandmarks on curves and surfaces**

Definition (Generalized Procrustes Analysis, GPA)

Procrustes shape coordinates $\mathbf{x}_{P,ij} = c_i \boldsymbol{\Gamma}_i (\mathbf{x}_{ij} - \mathbf{t}_i)$, where c_i is *scale*, $\boldsymbol{\Gamma}_i$ is *rotation matrix* and $\mathbf{t}_i$ is *translation*, $\mathbf{x}_{P,ij}$ are rows of $\mathbf{X}_{P,i}$, $i = 1, ..., n$. Then we say that $\mathbf{X}_i, i = 1, 2, ..., n$ are in *optimal position* or have ***the best Procrustes fit*** in the sense of 'shape' if

$$\arg\inf \sum_{1 \le i \le j \le n} \| \mathbf{X}_{P,i} - \mathbf{X}_{P,j} \|^2 =$$

$$\underbrace{\arg\inf}_{\substack{\boldsymbol{\Gamma}_1, \ldots \boldsymbol{\Gamma}_n \in SO(2) \\ \mathbf{t}_1, \ldots \mathbf{t}_n \in \mathbb{R}^d, , c_1, c_2, \ldots c_n \in \mathbb{R}^+}} \left\{ \sum_{1 \le i \le j \le n} \left\| c_i \boldsymbol{\Gamma}_i \left(\mathbf{X}_i - \mathbf{1}_k \mathbf{t}_i^T \right)^T - c_j \boldsymbol{\Gamma}_j \left(\mathbf{X}_j - \mathbf{1}_k \mathbf{t}_j^T \right)^T \right\|^2 \right\}$$

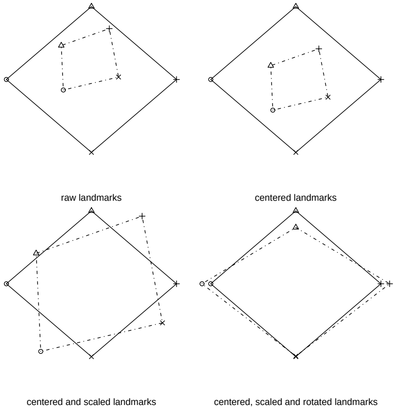

Figure: Procrustes Geometry

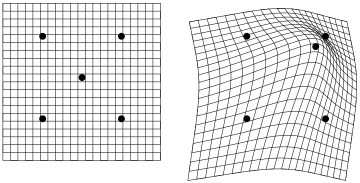

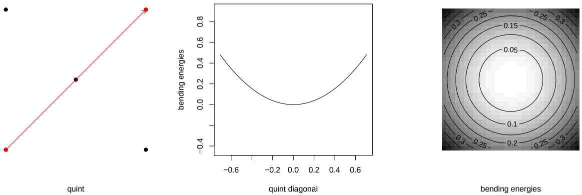

Figure: **TPS deformation grid**, **bending**, and **bending energy** $J(\mathbf{f})$

Traditional vs Geometric Morphometrics

Fish Neurocrania—*Rutilus rutilus* and *R.pigus* (Cyprinidae)

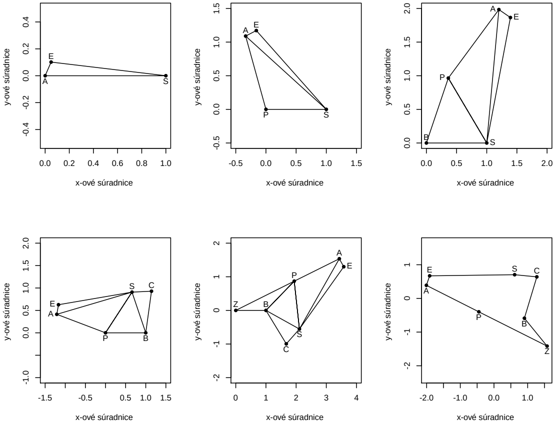

Figure: Sequential algorithm combining Triangle Geometry, Bookstein two-point registration

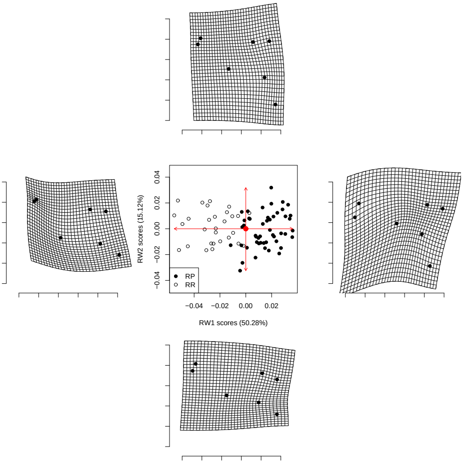

Figure: Model Choice—Shape Space PCA

Traditional vs Geometric Morphometrics

Fish Neurocrania—*Rutilus rutilus* and *R.pigus* (Cyprinidae)—Form Space PCA

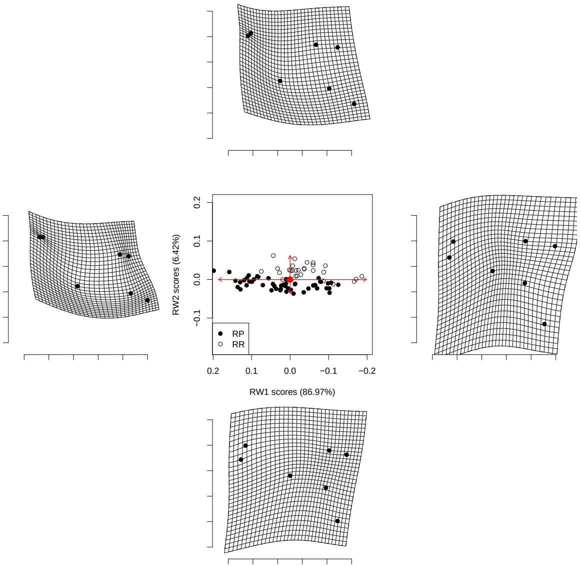

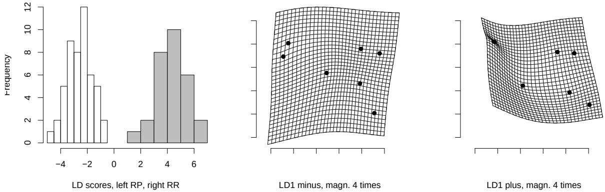

Frequency
0
2
4
6
8
10
12
−4
−2
0
2
4
6
LD scores, left RP, right RR
LD1 minus, magn. 4 times
LD1 plus, magn. 4 times

- **professionally digitised glass plate negatives of fossil skulls** (Předmostí 1 – P1, Předmostí 3 – P3, Předmostí 4 – P4, Předmostí 9 – P9, Předmostí 10 – P10)
- in the accessible norms: frontal, lateral sin., occipital, basal, and vertical views
- the skulls in question are those determined by Matiegka to have been females (P1, P4, P10) and males (P3, P9)
- **Katina, S.**, Sefcakova, A., Veleminska, J., Bruzek, J., Veleminska, P., 2004: A Geometric approach to cranial sexual dimorphism in the upper palaeolithic skulls from Předmostí (Upper Palaeolithic, Czech Republic). *Journal of the National Museum, Natural History Series* 173, 1–4:133–144

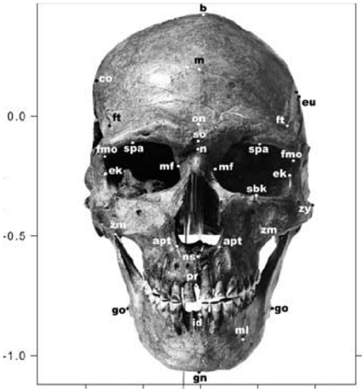

b
m
co
eu
0.0
ft
on
ft
so
fmo
spa
n
spa
fmo
mf
mf
ek
ek
sbk
zy
-0.5
zm
zm
apt
apt
ns
pr
go
go
id
ml
-1.0
gn

Skulls
Norma lateralis

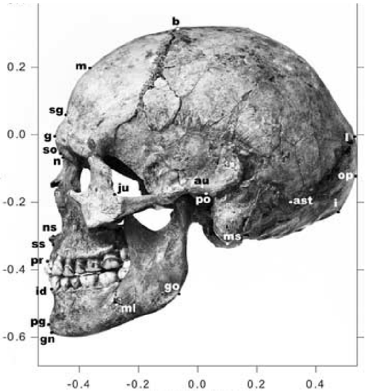

- lateral x-rays of the patients heads–**complete unilateral cleft of lip and palate** (UCLP)
- Velemínská J., **Katina, S.**, Šmahel, Z., Sedláčková, M., 2006: Analysis of facial skeleton shape in patients with complete unilateral cleft lip and palate: Geometric morphometrics. *Acta Chirurgiae Plasticae*, **48,1**: 26–32
- Velemínská J., Šmahel, Z., **Katina, S.**, 2006: Development prediction of sagittal intermaxillary relations in patients with complete unilateral cleft lip and palate during puberty. *Acta Chirurgiae Plasticae*, **49,2**: 41–46

UCLP

- 48 boys, complete unilateral cleft of lip and palate (UCLP), without symptoms of other associated malformations, Clinic of Plastic Surgery in Prague
- homogenously operated by the same team of surgeons (cheiloplasty according to Tennison, periosteoplasty without the nasal septum repositioning
- patients monitored during puberty, at the ages of 10 and 15 (born between 1972 and 1978)
- 22 landmarks (x-rays of the patients' heads, under standard conditions, SigmaScan Pro 5 software)

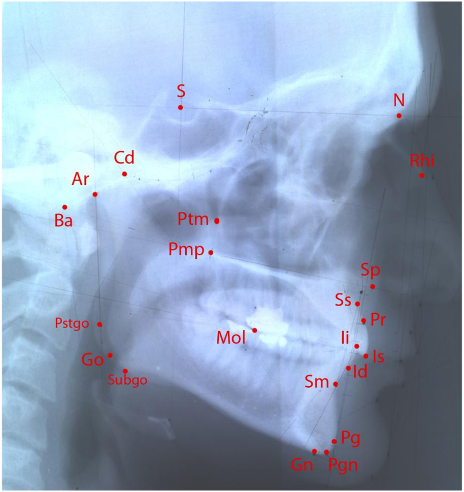
S
N
Cd
Rhi
Ar
Ba
Ptm
Pmp
Sp
Ss
Pr
Pstgo
Mol
Ii
Is
Go
Id
Subgo
Sm
Pg
Gn
Pgn

Figure: www.craniofacial.net

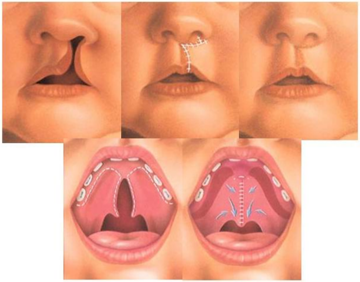

Figure: http://www.plasticsurgery.org

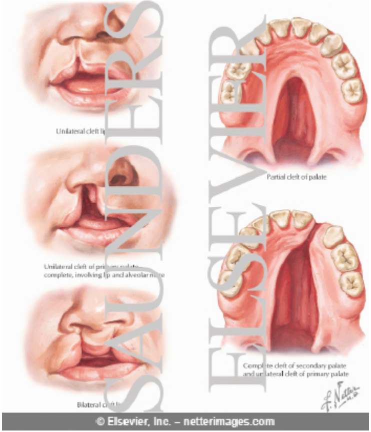

Figure: UCLP example

Morphology of human hand

- two-dimensional morphology of **human hand in palmar view**
- hands recorded as **digital images** (TIFF format, 24 colours, 150dpi, 100
- subjects—**100 females and 75 males**—recruited predominantly from population of college students of cities Brno and Ostrava (Czech Republic)
- **16 landmarks**
- Kralik, M., **Katina, S.**, 2014: Distal Part of the Human Hand: Study of Form Variations and Sexual Dimorphism using Geometric Morphometrics. Submitted

Morphology of human hand

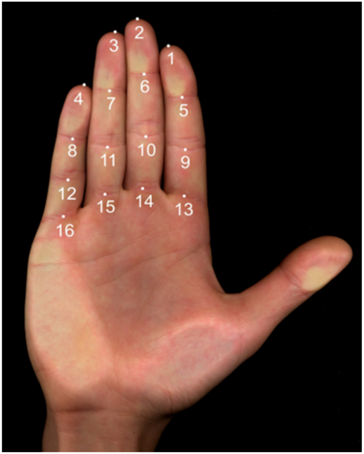

Eco-morpology of fishes

- Tomeček, J., Kovač, V., **Katina, S.**, 2005: Ontogenetic variability in external morphology of native (Canadian. and nonnative (Slovak. populations of pumpkinseed (Lepomis gibbosus, Linnaeus 1758. *Journal of Applied Ichthyology* **21**: 335–344
- Zahorska, E., Kovač, V, Falka, I., Beyer, K., **Katina, S.**, Copp, G.H., Gozlan, R., 2009: Morphological variability of the Asiatic cyprinid, topmouth gudgeon Pseudorasbora parva, in its introduced European range. *Journal of Fish Biology* **74**: 167–185
- Čapova, M., Zlatnicka, I., Kovač, V., **Katina, S.**, 2008. Ontogenetic variability in external morphology of monkey goby, Neogobius fluviatilis (Pallas, 1814) and its relevance to invasion potential. *Hydrobiologia* 607: 17–26
- Novomeska, A., **Katina, S.**, Copp, G.H., Pedicillo, G., Lorenzoni, M., Pompei, L., Cucherousset, J., Kovač, V., 2013: Morphological variability of black bullhead Ameiurus melas (Rafinesque, 1820) in its non-native European populations. *Journal of Fish Biology* 82, 4: 1103–1451

1. total length (1–2)
2. standard length (1–3)
3. head length (1–4)
4. preorbital distance (1–5)
5. eye diameter (5–6)
6. postorbital distance (6–4)
7. head depth (7–8)
8. predorsal distance (1–9)
9. preventral distance (1–10)
10. preanal distance (1–11)
11. postdorsal distance (12–3)
12. V–A distance (10–11)
13. D–A distance (9–11)
14. D–adip distance (9–13)
15. adipA distance (13–11)
16. adip – post. A distance (13-14)
17. post. adip – C fin base (15–3)
18. C peduncle length (14–3)
19. C peduncle depth (14–16)
20. minimum body depth (17–18)
21. body depth (9–19)
22. D-fin depth (9–20)
23. V-fin depth (10–21)
24. A-fin depth (22–23)
25. C-fin depth (24–25)
26. D-fin length (9–12)
27. adip length (13–15)
28. A-fin length (11–14)
29. C-fin length (2–3)
30. P-fin length (26–27)
31. interorbital distance(28–29)
32. head width (30–31)

Eco-morpology of fishes

Topmouth gudgeon (*Pseudorasbora parva*)

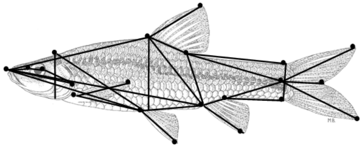

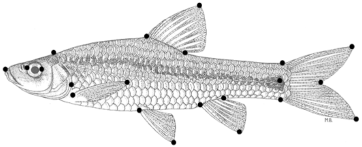

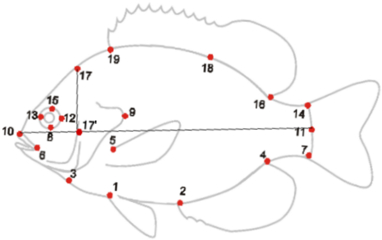

19
18
17
15
16
14
13
12
9
10
17'
8
11
5
6
4
7
3
1
2

Eco-morpology of fishes

Monkey goby (*Neogobius fluviatilis*)

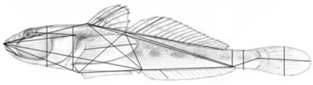

a

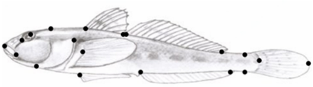

b

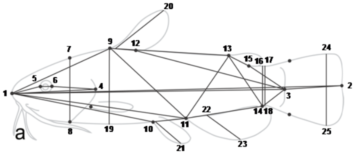

20
9
12
7
13
15
16
17
24
5
6
4
1
2
3
22
14
18
11
a
8
19
10
25
21
23

Skulls

- example re-uses *part of a Vienna data set of* 372 *skulls from various collections*
- 106 human crania (38 adult females, 54 males, 3 juvenile females, 11 juvenile males, 14 unknown sex; from newborns to adults)
- Dept. of Archaeological Biology and Anthropology, Natural History Museum, Vienna, Austria
- Dept. of Anthropology, University of Vienna, Vienna, Austria
- *Weisbach collection* - acquired and exhumed skeletons of soldiers of the Austro-Hungarian monarchy, sex and age of these crania are known from military records
- *Hallstatt collection* from ossuary in Hallstatt, sex and age are known from the church-books

Skulls

- data – 347 landmarks and semilandmarks – 32 landmark points, 7 ridge curves totalling 161 semilandmarks and 154 surface semilandmarks [5 – base, 184 – face, 158 – neurocranium]
- landmark points on **both sides** of every cranium and semilandmarks (on curves and surface) **on the left side** of every cranium were digitalized using a MicroScribe 3*DX* (Mitteroecker et al, 2004, Gunz, 2005)
- **Katina, S.**, Bookstein, FL., Gunz, P., Schaefer, K., 2007: Was it worth digitizing all those curves? A worked example from craniofacial primatology. *American Journal of Physical Anthropology* Suppl. **44**: 140.

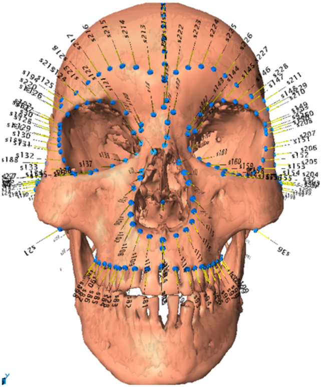

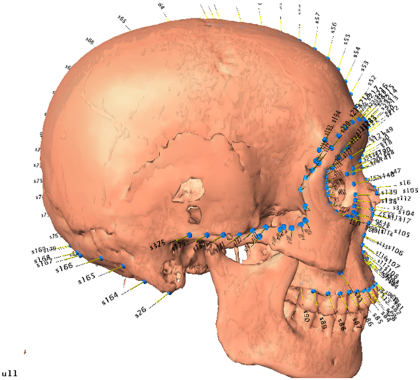
s166
s165
s164
s26
s16
s103
s104
s105
s106
ull

Skulls
Norma lateralis sin.

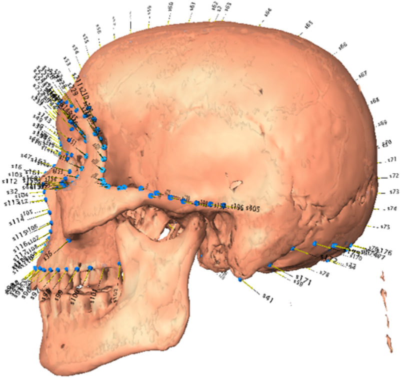

Skulls
Norma occipitalis

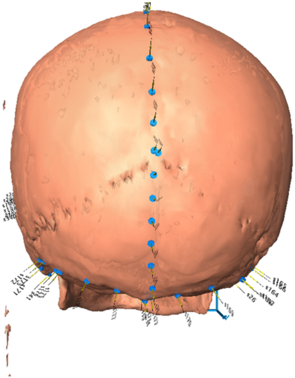

Skulls
Norma verticalis

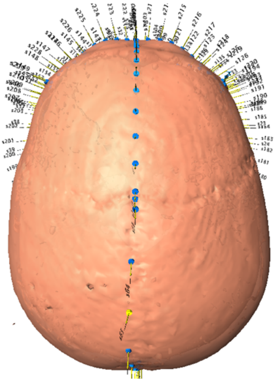

Skulls
Norma basilaris

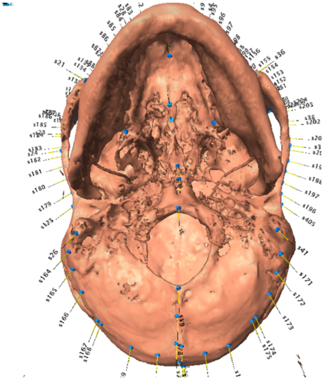

Growth of modern human mandible–3D, CTs

- CTs of 151 modern humans (78 females and 73 males) of mixed ethnicity, living in France, from birth to adulthood [Pellegrin Hospital (Bordeaux), Necker Hospital (Paris) and Clinique Pasteur (Toulouse)]
- each mandibular surface was reconstructed from the CT-scans via the software package **Amira** (Mercury Computer Systems, Chelmsford, MA)
- open-source software **Edgewarp3D** (Bookstein & Green 2002), a 3D-template of 415 landmarks and semilandmarks was created to measure the mandibular surface and was warped onto each mandible

- Coquerelle, M., Bayle, P., Bookstein, F.L. Braga, J., Halazonetis, D.J., **Katina, S.**, Weber, G.W., 2010: Covariation between dental development and mandibular form changes: a study combining additive conjoint measurement and geometric morphometrics. *Journal of Anthropological Sciences* **88**: 129-150

Growth of modern human mandible–3D, CTs

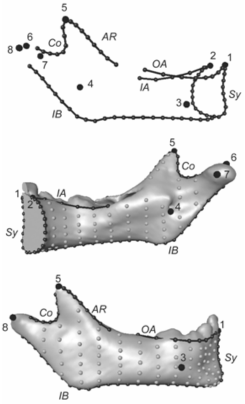

Tibial shape analysis–3D, CTs

- 77 tibiae of four extant primate species: *Homo sapiens*, *Gorilla gorilla*, *Pan troglodytes*, *Pongo pygmaeus*
- each tibial surface was reconstructed from the CT-scans via the software package **Rapidform 2006**
- 15 landmarks and 500 semilandmarks
- Frelat, M., **Katina, S.**, Weber, G.W., Bookstein, F.L., 2012: Technical note: A novel Geometric Morphometric approach to the study of long bone shape variation. *American Journal of Physical Anthropology* 149, 4: 628–638

Tibial shape analysis–3D, CTs

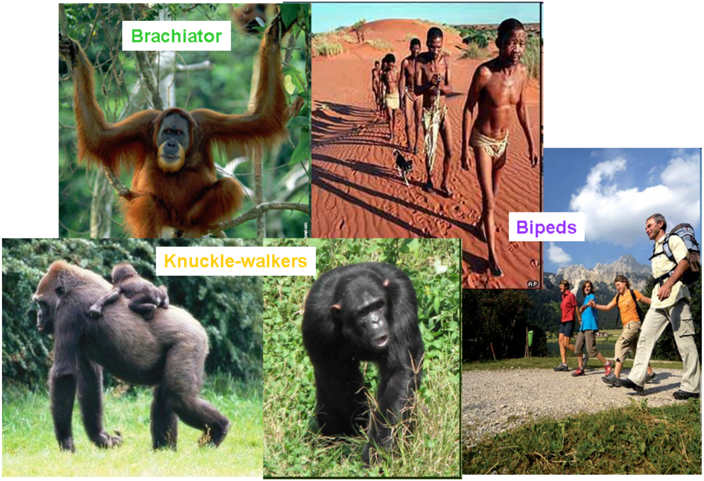

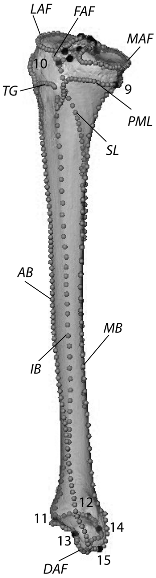

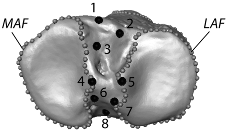

1: AMM
2: ALM
3: ACL
4: MIE
5: LIE
6: PMM
7: PLM
8: PCL
9: PMB
10: PSL
11: ALC
12: PLC
13: AMC
14: PMC
15: DDL

Human faces in 2D

- Oberzaucher, E., **Katina, S.**, Holzleitner, I.J., Schmehl, S.F., Mehu-Blantar, I., Grammer, K., 2012: The myth of hidden ovulation: Shape and texture changes in the face during the menstrual cycle. *Journal of Evolutionary Psychology* **10, 4**: 163–175
- Pflüger, L.S., Oberzaucher, E., **Katina, S.**, Holzleitner, I.J., Gramer, K., 2012: Cues to fertility: perceived attractiveness and facial shape predict reproductive success. *Evolution and Human Behaviour* **33, 6**: 108–114

Human faces in 2D

- 20 young women (aged between 19 and 31) who reported to have a regular menstrual cycle and did not take any hormonal contraceptives
- standardized facial photographs–one taken in the **ovulatory** and one in the **luteal phase**
- in a **forced choice task**, 50 male and 50 female subjects were presented with these photographs of each participant–to pick out the **more attractive, healthy, sexy, and likeable**, of the two
- skin patches sized 150 $\times$ 150 pixels from the **cheek** and subjected them to the same forced choice task with slightly modified adjectives

'Hidden' ovulation signals–2D, facial photographs

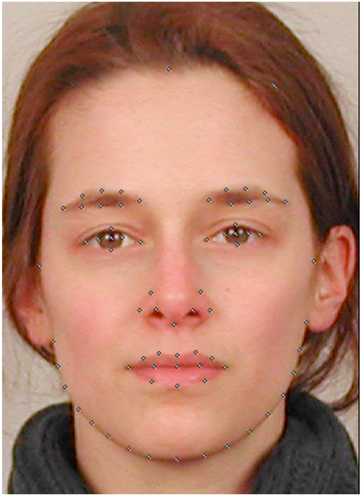

Folding of human cortex

- **MRI** and **BrainVisa** software
- human brain folding patterns – cortical folds of **central sulcus**
- 62 left and right curves following the bottom of central sulcus
- from 35 to 149 semilandmarks on the curves

Folding of human cortex

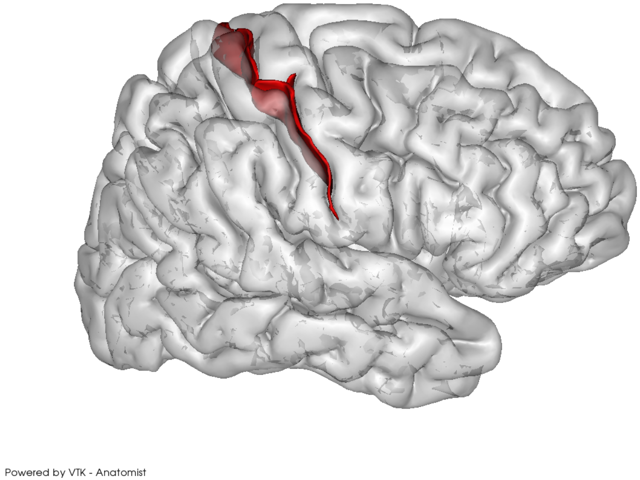

Human brain again

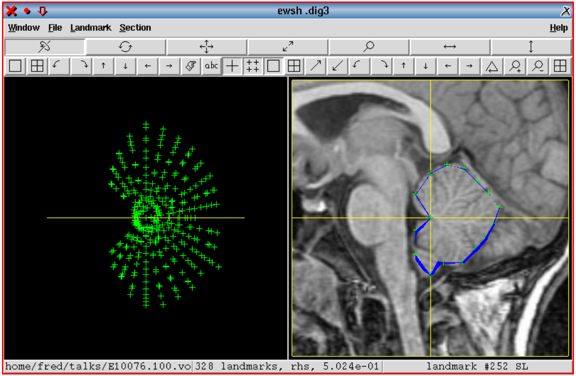

Human brain again

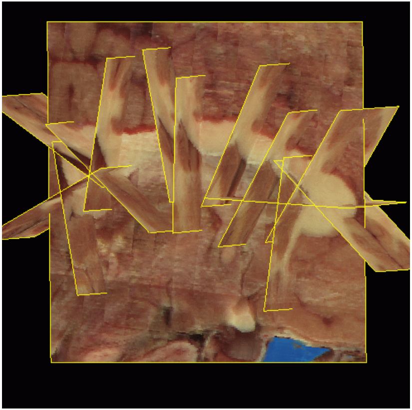

3D facial laser-scans – velocardiofacial syndrome

- 72 laser-scans of human faces
- 45 velo-cardio-facial syndrome (**VCFS**; chromosome 22 deletion syndrome associated with very high risk of schizophrenia?like psychosis; 25 females and 20 males)
- 27 controls (14 females and 13 males; siblings or closed relatives of similar age)
- from these, after coupling, it remains 42 **pairs** (also after exclusion of several laser-scans with low quality)
- 23 **biologically homologous anatomical landmarks** and 1664 **geometrically homologous semilandmarks on curves and surface patches**
- **mesh** of 59242 points triangulated by 117386 **faces (triangulated mesh)**

3D facial laser-scans

VCFS - -Royal College of Surgeons, Dublin, Ireland

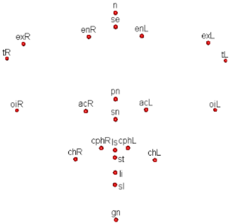

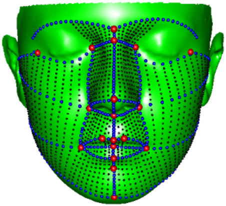

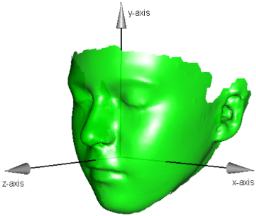

3D face—stereo-camera campture

Control data—Dental clinic, The University of Glasgow, UK

A **triangle mesh** $\mathcal{M}_i, i = 1, 2, \ldots n$, consists of

- a set of **vertices** $\mathcal{V}_i = \{v_{i1}, v_{i2}, \ldots, v_{iV}\}$
- a set of **triangular faces** connecting them $\mathcal{F}_i = \{f_{i1}, f_{i2}, \ldots, f_{iF}\}, f_j \in \mathcal{V}_i \times \mathcal{V}_i \times \mathcal{V}_i$
- a set of **edges** $\mathcal{E}_i = \{e_{i1}, e_{i2}, \ldots, e_{iE}\}, e_j \in \mathcal{V}_i \times \mathcal{V}_i$
- **a 3D position** $\mathbf{p}_j$ to each vertex $v_j \in \mathcal{V}$

  $$\mathcal{P} = \{\mathbf{p}_{i1}, \mathbf{p}_{i2}, \ldots, \mathbf{p}_{iV}\}, \mathbf{p}_j = \mathbf{p}(v_j) = \begin{pmatrix} x(v_j) \\ y(v_j) \\ z(v_j) \end{pmatrix} \in \mathbb{R}^3, \text{ such}$$

  that each face $f \in \mathcal{F}_i$ corresponds to a triangle in 3D space specified by its three vertex position

A **configuration matrix**

$$\mathbf{X}_i = \left(\mathbf{x}_i^{(1)}, \mathbf{x}_i^{(2)}, \mathbf{x}_i^{(3)}\right),\ \mathbf{x}_i^{(\cdot)} = (x_{i1}^{(\cdot)}, x_{i2}^{(\cdot)}, \ldots, x_{ik}^{(\cdot)})^T,\ k \ll V$$

$$\mathbf{X}_i = (\mathbf{x}_{i1}, \mathbf{x}_{i2}, \ldots, \mathbf{x}_{ik})^T,\ \mathbf{x}_{ij} = (x_{ij}^{(1)}, x_{ij}^{(2)}, x_{ij}^{(3)})^T, j = 1, 2, \ldots, k$$

The **(semi)landmarks** $\mathbf{x}_{ij}$

- k_1 **landmarks**
- k_2 **semilandmarks on curve** $(k_{21}, k_{22}, \ldots, k_{2C})$
- k_3 **semilandmarks on surface** $(k_{31}, k_{32}, \ldots, k_{3S})$

Definition (Affine and non-affine coordinates)

Regressing each $k \times d$ matrix $\mathbf{X}_{P,i}$ ($d = 2, 3$) onto the $\overline{\mathbf{X}}_P$ can be defined by the *MMLRM* (***Multivariate Multiple Linear Regression Model***)

$$\mathbf{X}_{P,i} = \overline{\mathbf{X}}_P \beta_i + \epsilon_i; \widehat{\beta}_i = \left(\overline{\mathbf{X}}_P^T \overline{\mathbf{X}}_P\right)^{-1} \overline{\mathbf{X}}_P^T \mathbf{X}_{P,i}, i = 1, 2, ...n.$$

Let $\widehat{\beta}_i = \left(\widehat{\beta}_{i1} \vdots \widehat{\beta}_{i2}\right)$ for 2D and $\widehat{\beta}_i = \left(\widehat{\beta}_{i1} \vdots \widehat{\beta}_{i2} \vdots \widehat{\beta}_{i3}\right)$ for 3D, then

1. **affine Procrustes coordinates**: $\mathbf{X}_{A,i} = \mathbf{X}_{P,i} \widehat{\beta}_i$
2. **non-affine Procrustes coordinates** (residuals of *MMLRM*): $\mathbf{X}_{NA,i} = \overline{\mathbf{X}}_P + \left(\mathbf{X}_{P,i} - \mathbf{X}_{A,i}\right)$

Example (IM 1 a PRM 1)

Majme interpolačný model [IM1] ($f:\mathbb{R}\rightarrow\mathbb{R}$)

$$\begin{pmatrix}\mathbf{y}\\0\\0\end{pmatrix}=\mathbf{X}\beta,\mathbf{X}=\begin{pmatrix}\mathbf{S}&\mathbf{1}_k&\mathbf{x}\\\mathbf{1}_k^T&0&0\\\mathbf{x}^T&0&0\end{pmatrix},\beta=\begin{pmatrix}\mathbf{w}\\c\\a\end{pmatrix}$$

kde $\mathbf{x}_{k\times 1}=(x_1,...,x_k)^T$, $\mathbf{y}_{k\times 1}=(y_1,y_2,...,y_k)^T$, $(\mathbf{S})_{ij}=\phi(x_i,x_j)=\frac{1}{12}|x_i-x_j|^3$.
Majme penalizovaný regresný model [PRM1] ($f:\mathbb{R}\rightarrow\mathbb{R}$)

$$\mathbf{y}_P=\begin{pmatrix}\mathbf{y}\\\mathbf{0}_{k+2}\end{pmatrix}=\mathbf{X}_P\beta+\epsilon,\mathbf{X}_P=\begin{pmatrix}\mathbf{X}_{\text{dm}}\\\sqrt{\lambda}\mathbf{R}\end{pmatrix},\mathbf{S}_P=\begin{pmatrix}\mathbf{0}_{2\times 2}&\mathbf{0}_{2\times k}\\\mathbf{0}_{k\times 2}&\mathbf{S}\end{pmatrix},$$

kde $\mathbf{X}_{\text{dm}}=(\mathbf{1}_k\vdots\mathbf{x}\vdots\mathbf{S})$ je **penalizovaná časť matice plánu**, $(\mathbf{S})_{ij}=\phi(x_i,x_j)=\frac{1}{12}|x_i-x_j|^3$, $\mathbf{S}_P=\mathbf{R}^T\mathbf{R}$ a $\sqrt{\lambda}\mathbf{R}$ je **penalizovaná časť matice plánu**. Potom penalizovanú sumu štvorcov budeme písať v tvare $SS_{\text{pen}}=(\mathbf{y}-\mathbf{X}_{\text{dm}}\beta)^T(\mathbf{y}-\mathbf{X}_{\text{dm}}\beta)+\lambda\beta^T\mathbf{S}_P\beta=\mathbf{y}^T\mathbf{y}-2\beta^T\mathbf{X}_{\text{dm}}^T\mathbf{y}+\beta^T(\mathbf{X}_{\text{dm}}^T\mathbf{X}_{\text{dm}}+\lambda\mathbf{S}_P)\beta$.

Example (IM 1)

Majme interpolačný model [IM1] a krivku **X** definovanú bodmi $(x_j^{(1)}, x_j^{(2)})$, kde $j = 1, 2, \ldots k$ a **X** je matica rozmerov $k \times 2$. Nech $\mathbf{d}_{ch}$ je vektor k **chordálnych (uhlových) vzdialeností**, kde $d_{ch}^{(j)}$ zodpovedá vzdialenosti bodov $(x_{j-1}^{(1)}, x_{j-1}^{(2)})$ a $(x_j^{(1)}, x_j^{(2)})$ krivky **X**, $j = 2, 3, \ldots k$; $d_{ch}^{(1)} = 0$. IM1 je počítan pre $(d_{ch}^{(j)}, x_j^{(1)})$ a $(d_{ch}^{(j)}, x_j^{(2)})$; $j = 1, 2, \ldots k$ osobitne; vizualizujeme krivku $\widehat{\mathbf{X}}$ s k odhadnutými bodmi, kde j-ty bod je rovný $(\widehat{x}_j^{(1)}, \widehat{x}_j^{(2)})$, $j = 1, 2, \ldots k_I \geq k$. **X** sa nazýva **resamplovaná interpolovaná krivka X**.

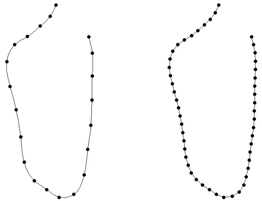

Example (IM 3)

Majme interpolačný model [IM3; thin-plate splajn, TPS] ($f : \mathbb{R}^2 \to \mathbb{R}^2$)

$$\begin{pmatrix} \mathbf{Y} \\ \mathbf{0} \\ \mathbf{0} \end{pmatrix} = \begin{pmatrix} \mathbf{S} & \mathbf{1}_k & \mathbf{X} \\ \mathbf{1}_k^T & 0 & \mathbf{0} \\ \mathbf{X}^T & \mathbf{0} & \mathbf{0} \end{pmatrix} \begin{pmatrix} \mathbf{W} \\ \mathbf{c}^T \\ \mathbf{A} \end{pmatrix},$$

kde $\mathbf{X} = (\mathbf{x}_1, \dots \mathbf{x}_k)^T$ a $\mathbf{Y} = (\mathbf{y}_1, \dots \mathbf{y}_k)^T$, $(\mathbf{S})_{ij} = \phi(\mathbf{x}_i - \mathbf{x}_j)$, $\phi(\mathbf{x}) = \|\mathbf{x}\|_2^2 \log\left(\|\mathbf{x}\|_2^2\right)$, $\forall \|\mathbf{x}\|_2 > 0$, ak $\|\mathbf{x}\|_2 = 0$, potom $\phi(\mathbf{x}) = 0$. Potom extrapolácia IM3 bude definovaná ako $\mathbf{Y}_l \longmapsto \mathbf{X} + l \times (\mathbf{X} - \mathbf{Y})$, kde $l \in \mathbb{R}$.

TPS používame aj ako zobrazovaciu metódu, kedy hovoríme o **(ne)deformovanej štvorcovej TPS sieti** – kde ide o (nedeformovanú) štvorcovú sieť pre model $f : \mathbf{X} \longmapsto \mathbf{X}$ a deformovanú štvorcovú sieť pre model $f : \mathbf{X} \longmapsto \mathbf{Y}_l$. Ide v podstate o IM3 definovaný pre všetky uzly siete, kde $\mathbf{y}_j = \mathbf{f}(\mathbf{x}_j), j = 1, \ldots n_{cp}$; n_{cp} (*cp* znamená ”crossing points”) je počet uzlov siete (je jednoduché model predefinovať na (ne)deformovanú obdĺžnikovú TPS sieť). V TPS $f : \mathbf{X} \longmapsto \mathbf{Y}_l$ sa použijú odhadnuté koeficienty **W**, **c** a **A** na interpolovanie uzlov siete. Jednotlivé uzly sú potom pospájané (v smere oboch osí pre rovnaké j) *lokálne lineárne* (úsečkami) alebo *interpolovanou krivkou* (použitím IM1).

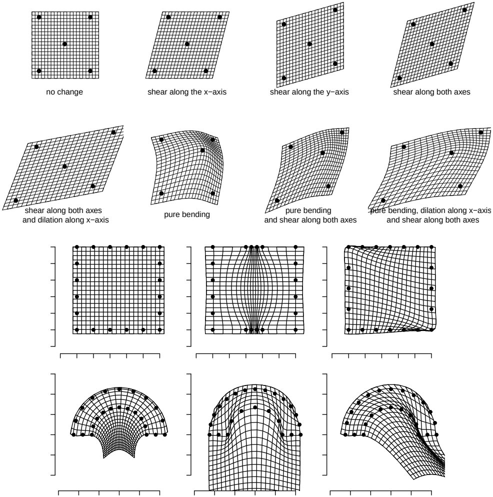

Figure: Affine, non affine-deformations, geometrical homology

Definition (Relative Warp Analysis (RWA))

If bending energy matrix $\mathbf{B}_e$ is calculated for the mean shape $\overline{\mathbf{X}}_P$, then $dk \times dk$ matrix $\mathbf{B} = \mathbf{I}_{d \times d} \otimes \mathbf{B}_e$. Let ***Generalized covariance matrix with respect to bending energy*** is equal to

$$\mathbf{S}_B^{(\alpha)} = \left(\mathbf{B}^-\right)^{\alpha/2} \mathbf{S} \left(\mathbf{B}^-\right)^{\alpha/2},$$

where $\left(\mathbf{B}^-\right)^{\alpha/2} = \sum_j \widehat{\lambda}_j^{-\alpha/2} \widehat{\gamma}_j^T \widehat{\gamma}_j$ is *Moore-Penrose generalized inverse* of $\mathbf{B}^{\alpha/2}$.The non-zero eigenvalues of $\mathbf{S}_B^{(\alpha)}$ calculated by SVD are $\widehat{l}_j$ and corresponding eigenvectors $\widehat{\mathbf{g}}_j$ (***relative warps, RW***). Then ***RW scores***

$$r_{ij} = \widehat{\mathbf{g}}_j^T \left(\mathbf{B}^-\right)^{\alpha/2} Vec\left(\mathbf{X}_{S,i}\right), i = 1, 2, ...n; j = 1, 2, ...J_d,$$

where J_d is the number of non-zero eigenvalues ($d = 2, 3$).

Definition (Relative Warp Analysis (RWA), cont.)

The effect of the jth RW can be viewed by plotting

$$Vec\left(\mathbf{X}_P\left(c, j, \alpha\right)\right) = Vec(\overline{\mathbf{X}}_P) \pm c_j \mathbf{B}^{\alpha/2} \widehat{\mathbf{g}}_j \widehat{l}_j^{1/2}, r_j = c_j \widehat{l}_j^{1/2}$$

for various values of $r_j \in \langle 0, \max(|r_{ij}|) \rangle$ (or reasonable magnification of $\max(|r_{ij}|)$; alternatively, either $c_j \sim N(0, 1)$ or fixing $c_j = 1$, magnification of $\widehat{l}_j^{1/2}$, standard deviation of RW_j scores), where $\mathbf{B}_e^{\alpha/2} = \sum_j \widehat{\lambda}_j^{\alpha/2} \widehat{\gamma}_j \widehat{\gamma}_j^T$. To emphasize

1. *large scale variability (global bending)*, $\alpha = 1$,
2. *small scale variability (local bending)*, $\alpha = -1$,
3. $\alpha = 0$, then we take $\mathbf{B}^0 = \mathbf{I}$ as the $dk \times dk$ identity matrix and the procedure is equivalent to <u>*PCA of Procrustes* shape coordinates</u>

Definition (Relative Warp Analysis (RWA), cont.)

1. ***Affine* contribution** to the variability by performing affine subspace *PCA* on the covariance matrix $\mathbf{S}_A$ of $n \times dk$ matrix $\mathbf{X}_A$ with the rows $Vec\left(\mathbf{X}_{A,i}\right)$, $i = 1, 2, ...n$ (which is equivalent to the *RWA* with $\alpha = 0$)
2. ***Non-affine* contribution** to the variability by performing non-affine subspace *PCA* on the covariance matrix $\mathbf{S}_{NA}$ of $n \times dk$ matrix $\mathbf{X}_{NA}$ with the rows $Vec\left(\mathbf{X}_{NA,i}\right)$, $i = 1, 2, ...n$
3. ***Contribution of (a)symmetry*** by augmenting relabeled and reflected Procrustes configurations to vectorized matrix of Procrustes shape coordinates and performing SVD of $\mathbf{S}_{AS}$
4. ***Size contribution*** by augmenting vectorized matrix of Procrustes shape coordinates by column of **centroid sizes** $\mathbf{x}_{size} = (\ln(CS_1), ..., \ln(CS_n))^T$, where $CS_i = \sqrt{(\sum_{j=1}^{k} \|\mathbf{x}_{ij} - \overline{\mathbf{x}}_i\|_2^2)} = \|\mathbf{X}_i\| = tr(\mathbf{X}_i\mathbf{X}_i^T)$, then $n \times (dk + 1)$ matrix of **vectorized form coordinates** $\mathbf{X}_F = (\mathbf{X}_S \vdots \mathbf{x}_{size})$, and finally performing SVD of $\mathbf{S}_F$

Data—human faces in 2D

- Oberzaucher, E., **Katina, S.**, Holzleitner, I.J., Schmehl, S.F., Mehu-Blantar, I., Grammer, K., 2012: The myth of hidden ovulation: Shape and texture changes in the face during the menstrual cycle. *Journal of Evolutionary Psychology* **10, 4**: 163–?175
- Pflüger, L.S., Oberzaucher, E., **Katina, S.**, Holzleitner, I.J., Gramer, K., 2012: Cues to fertility: perceived attractiveness and facial shape predict reproductive success. *Evolution and Human Behaviour* **33, 6**: 108–?114
- 20 young women (aged between 19 and 31) who reported to have a regular menstrual cycle and did not take any hormonal contraceptives
- standardized facial photographs–one taken in the **ovulatory** and one in the **luteal phase**
- in a **forced choice task**, 50 male and 50 female subjects were presented with these photographs of each participant–to pick out the **more attractive, healthy, sexy, and likeable**, of the two
- skin patches sized 150 $\times$ 150 pixels from the **cheek** and subjected them to the same forced choice task with slightly modified adjectives
- 46 **landmarks** and 26 **semilandmarks**

Data—human faces in 2D
2D Facial Analysis—two group differences

20 young women, $19-31$yrs old, $46+26$ (semi)landmarks

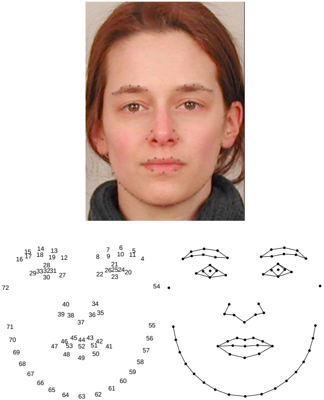

Figure: Design of facial (semi)landmarks

[Dpt. of Anthropology, University of Vienna, Vienna, Austria]

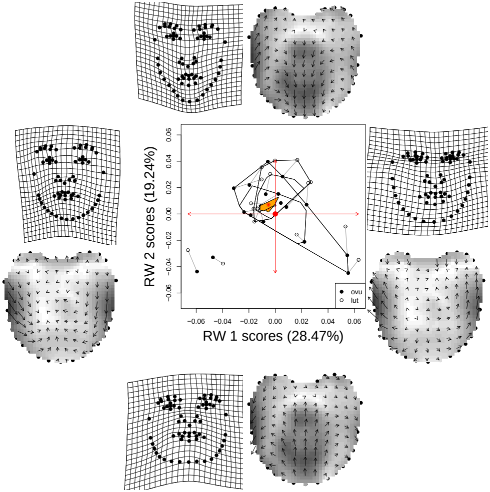

Figure: ***Shape*** space PCA—RWA of **S** (RW_1,RW_2 subspace)

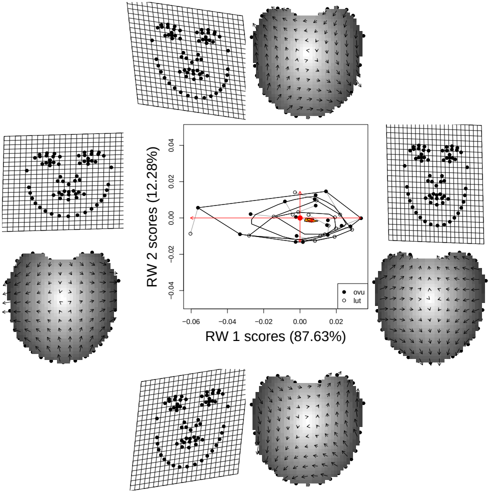

Figure: ***Affine*** subspace PCA—RWA of $\mathbf{S}_A$ (RW_1,RW_2 subspace)

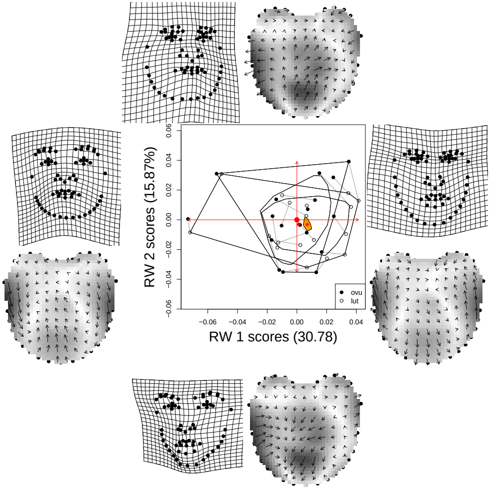

Figure: ***Nonaffine*** space PCA—RWA of $\mathbf{S}_{AN}$ (RW_1,RW_2 subspace)

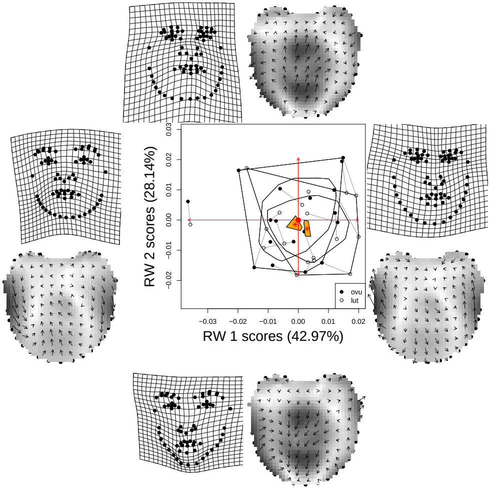

Figure: ***Nonaffine*** space PCA—RWA of $\mathbf{S}_B^{(1)}$ (RW_1,RW_2 subspace)

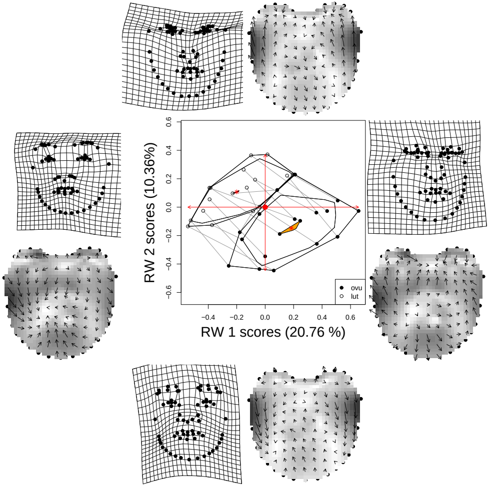

Figure: ***Nonaffine*** space PCA—RWA of $\mathbf{S}_B^{(-1)}$ (RW_1,RW_2 subspace)

Results of RWA—estimated shapes, RW1 and RW2

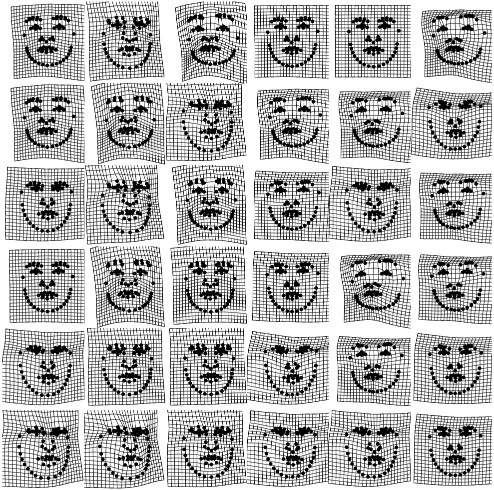

Geometric Morphometrics

2D Facial Analysis—searching biological signal in the data

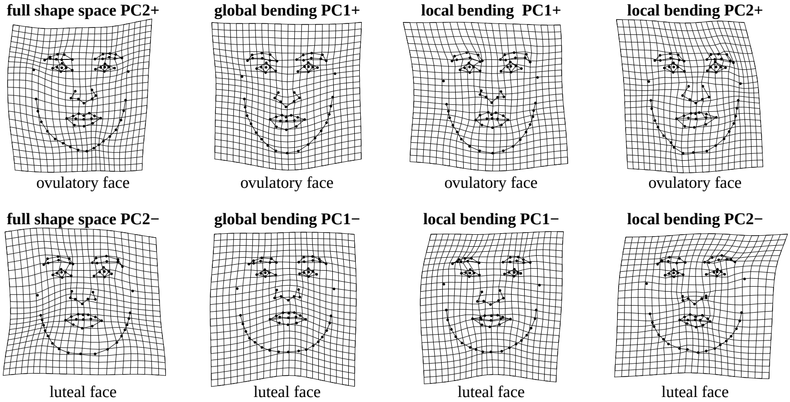

Figure: Summary of RWA/PCA analyses in all subspaces of ***paired shape differences*** [statistically significant RWs/PCs]

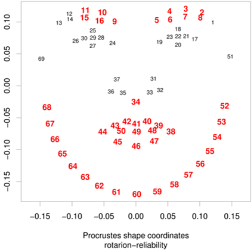

Figure: Head tilt vs reliability

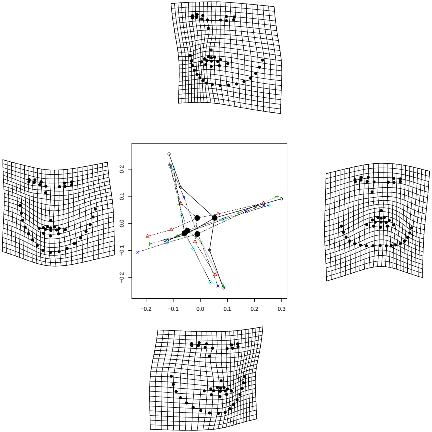

Figure: Head tilt PCA

Data—human faces in 2D

2D Facial Analysis—rural sample

Figure: Do we have other choice?

Data—human faces in 2D

2D Facial Analysis—rural sample

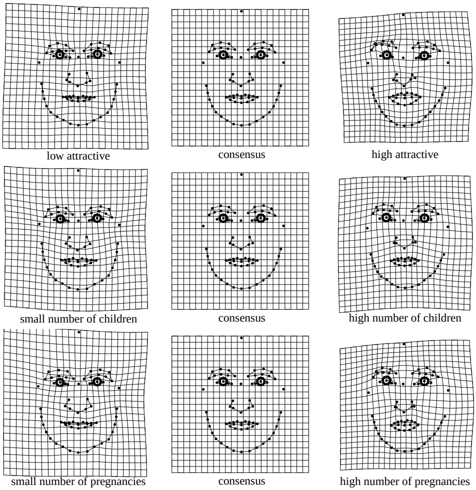

Figure: Do we have other choice?

Eco-morpology of fishes

Black bullhead (*Ameiurus melas*)

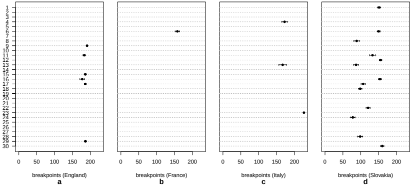

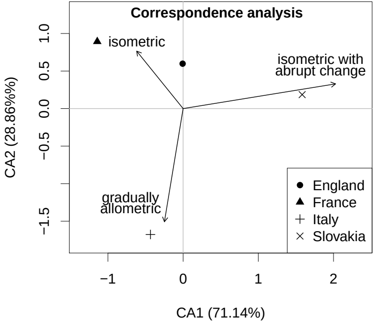

Eco-morpology of fishes

Black bullhead (*Ameiurus melas*)

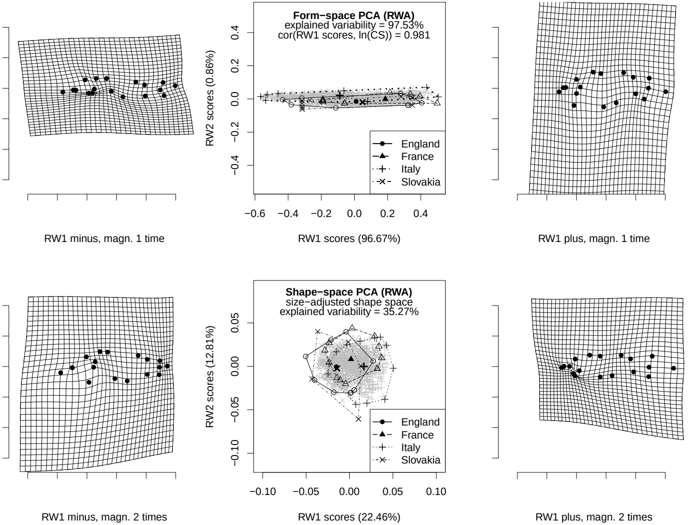

Eco-morpology of fishes

Black bullhead (*Ameiurus melas*)

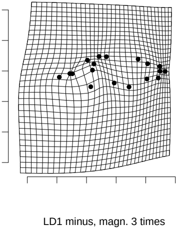

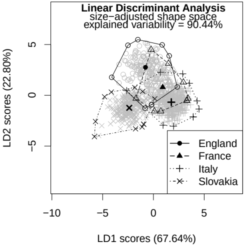

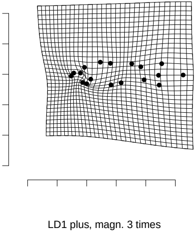

Eco-morpology of fishes

Black bullhead (*Ameiurus melas*)

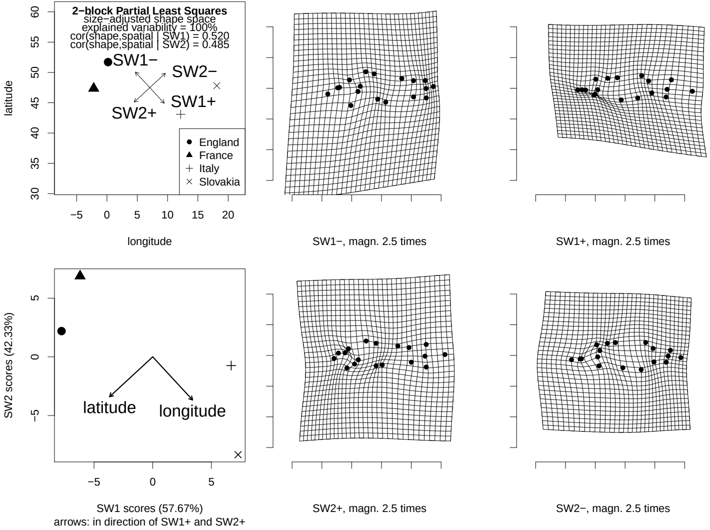

Figure: Originálny obraz metakarpu ľudskej ruky

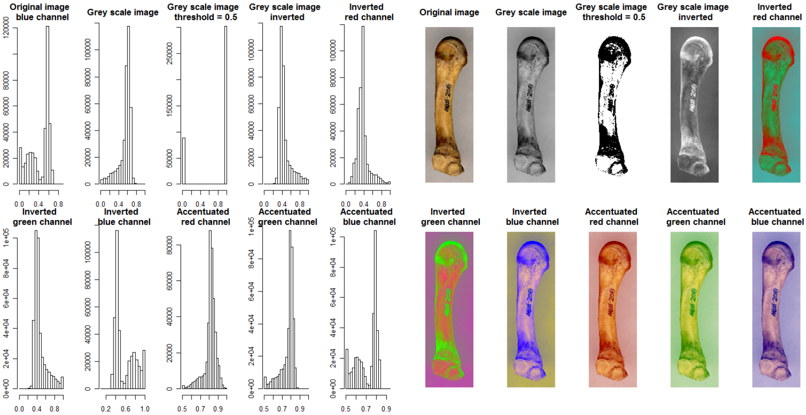

Figure: Histogramy rôznych transformácií farebných komponentov obrazu a nim zodpovedajúce obrazy metakarpu ľudskej ruky

Human Hand
Closed outline

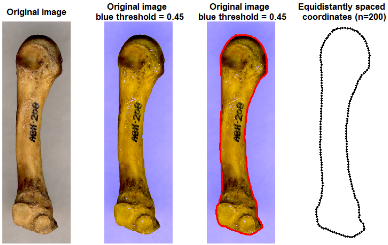

Figure: Extrahovaný obrys metakarpu ľudskej ruky

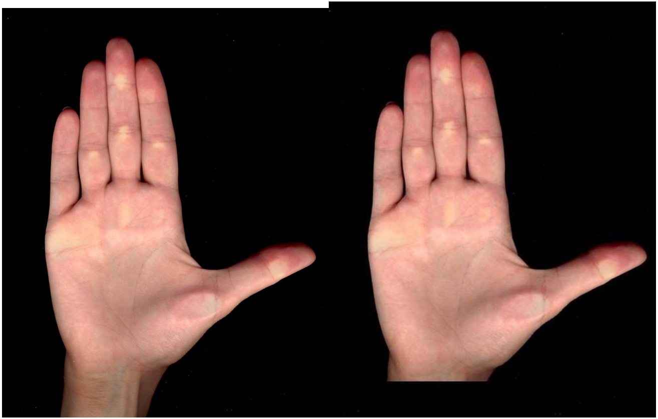

Figure: Obraz ľudskej ruky

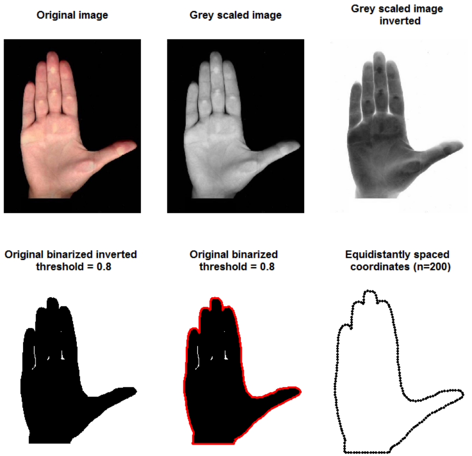

Figure: Extrakcia obrysu ľudskej ruky z vedeckej fotografie

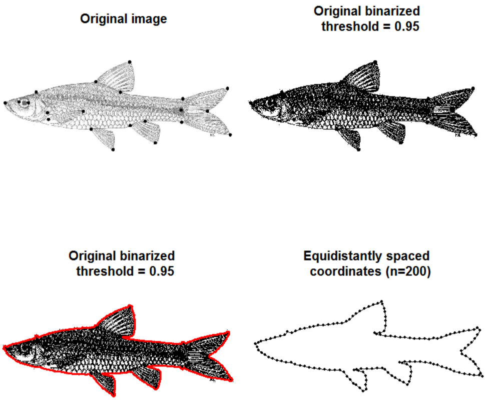

Figure: Extrakcia obrysu hrúzovca sieťovaného (*Pseudorasbora parva*)

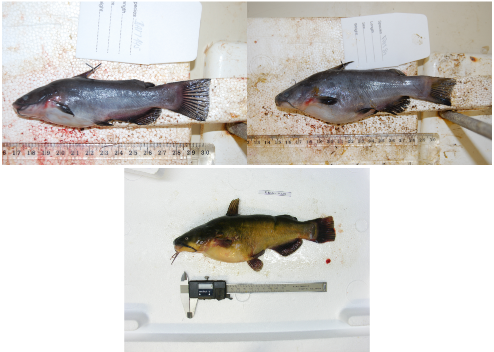

Figure: Extrakcia sumčeka čierneho (*Ameiurus melas*) z pozadia vedeckej fotografie

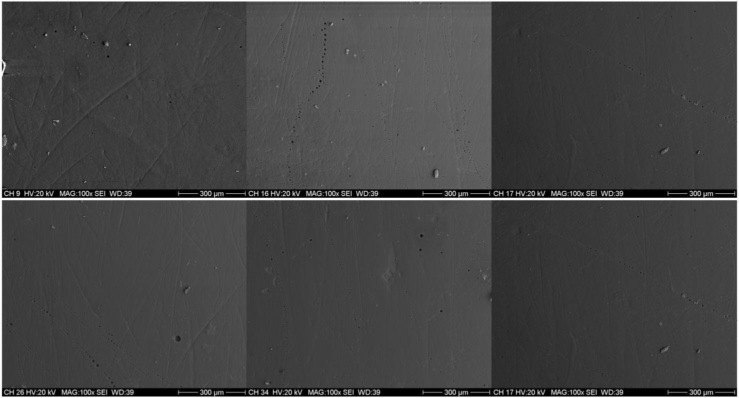
CH 9 HV:20 kV MAG:100x SEI WD:39
300 µm
CH 16 HV:20 kV MAG:100x SEI WD:39
300 µm
CH 17 HV:20 kV MAG:100x SEI WD:39
300 µm
CH 26 HV:20 kV MAG:100x SEI WD:39
300 µm
CH 34 HV:20 kV MAG:100x SEI WD:39
300 µm
CH 17 HV:20 kV MAG:100x SEI WD:39
300 µm

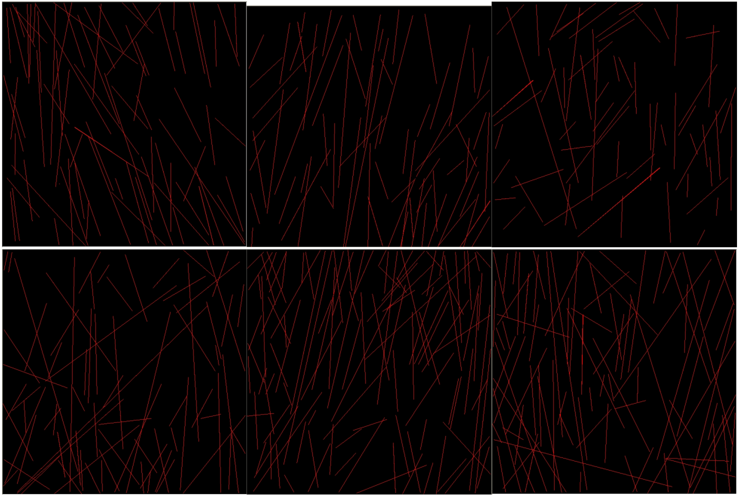

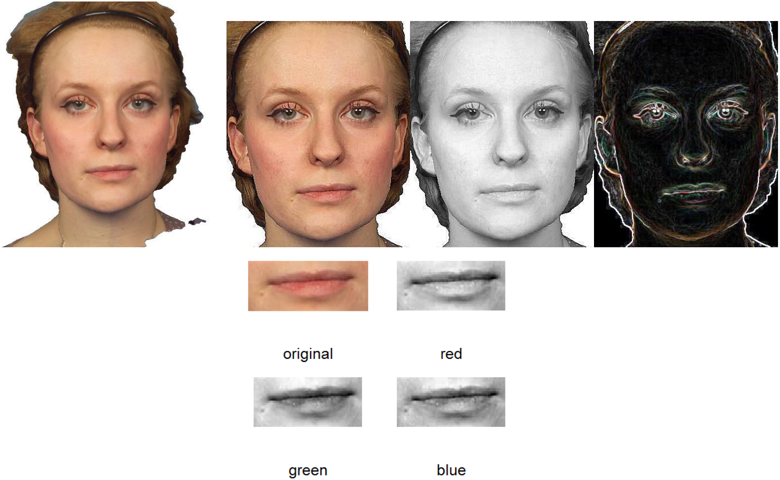

Figure: Image Processing of intensity in RGB space—2D example

Tibial shape analysis–3D, CTs

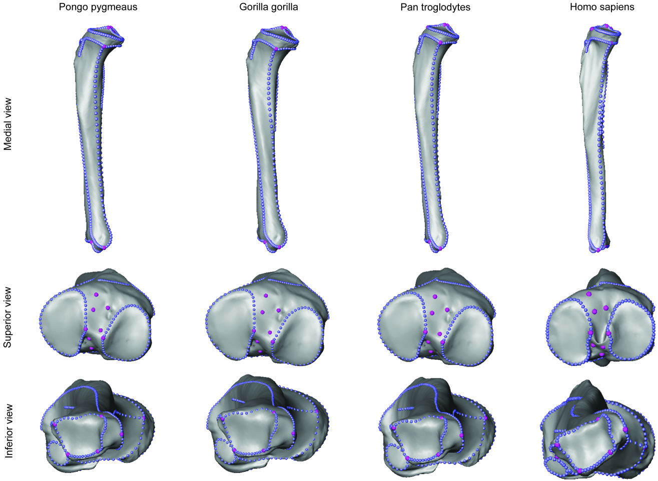

Tibial shape analysis–3D, CTs

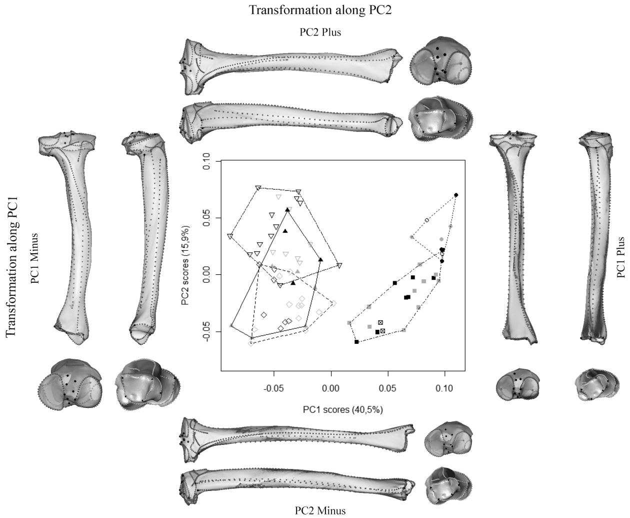

Tibial shape analysis–3D, CTs

(a) grand mean shape in the original geometry

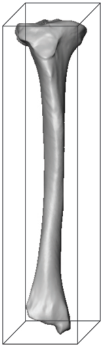

(b) grand mean shape in the fake nonaffine version

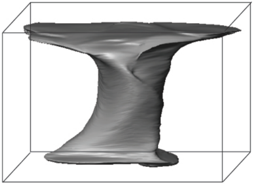

Tibial shape analysis–3D, CTs

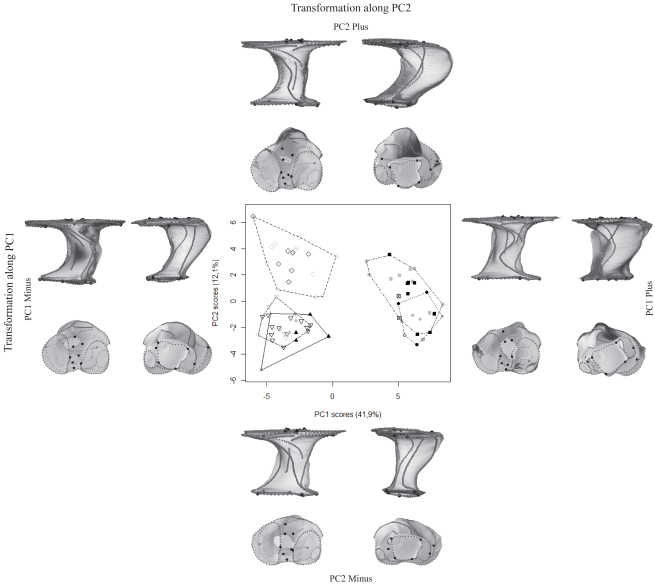

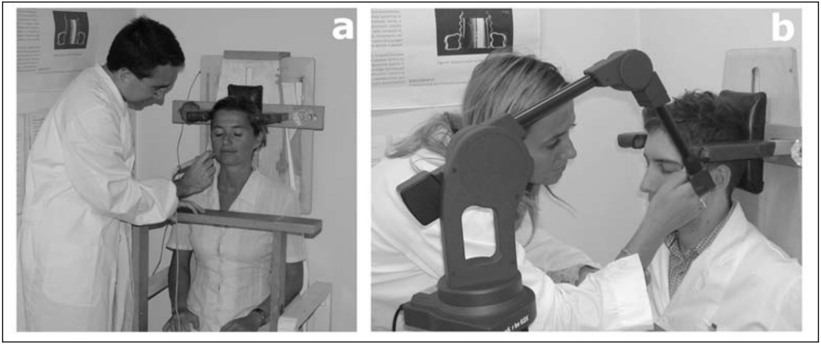

Figure: Why not?

3D laser-scan capture

3D facial shape—VCFS data, differences between cases and controls (paired data)

42 pairs of laser-scanned faces

$\approx$ 60000 mesh-points triangulated with 120000 faces

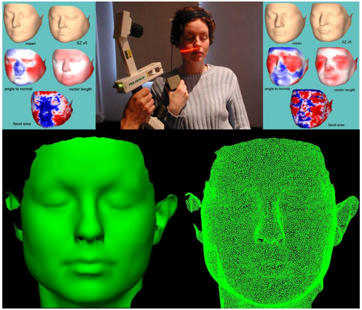

Royal College of Surgeons in Ireland, Dublin; **Face 3D data**

FastSCAN^{TM} Polhemus handheld 3D laser scanner

Why we study the VCFS faces?

- **multiple abnormalities**; extensive and variable phenotype that includes psychiatric disorders and craniofacial dysmorphology
- **increased risk for psychotic illness** [$\approx$ 25-fold]; second only to having an affected monozygotic co-twin $\approx$ 45-fold]
- **schizophrenia** characterised by subtle craniofacial dysmorphology that reflects underlying disturbance in early brain development
- To what extent is craniofacial dysmorphology in VCFS similar to or different from that evident in schizophrenia?
- OVER EARLY FETAL LIFE THE BRAIN AND FACE DEVELOP IN EXQUISITE EMBRYOLOGICAL INTIMACY

3D stereo-camera capture

System of 3D cameras—School of Maths & Stats, The University of Glasgow, UK

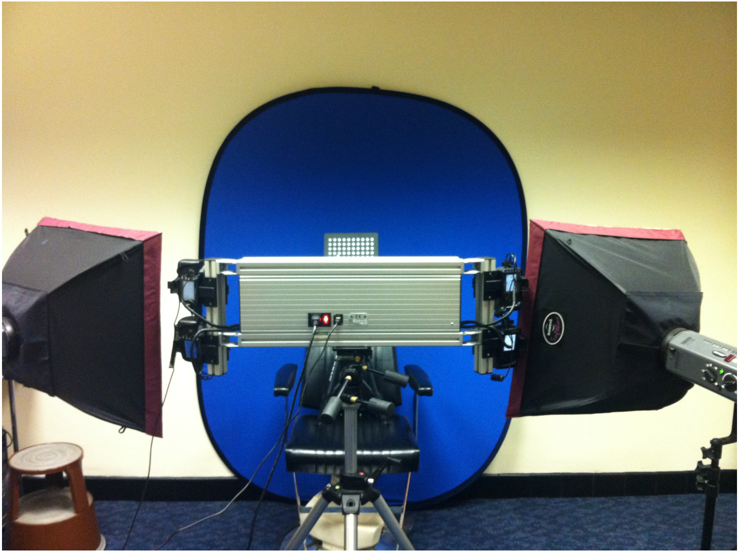

Di3D camera system

$\approx$ 300 stereo-photogrammetric images
$\approx$ 150000 mesh-points triangulated with 300000 faces

School of Maths & Stats, The University of Glasgow, UK; **Face 3D data**
Di3D camera system

3D stereo-camera capture
3D facial shape—image quality

3D stereo-camera capture
3D facial shape—image quality

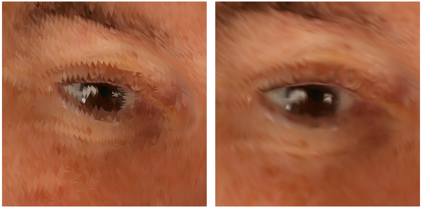

the effect of flat and smooth shading

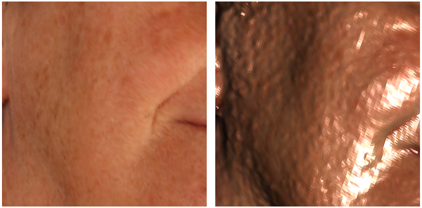

the effect of lighting calculation in geometry

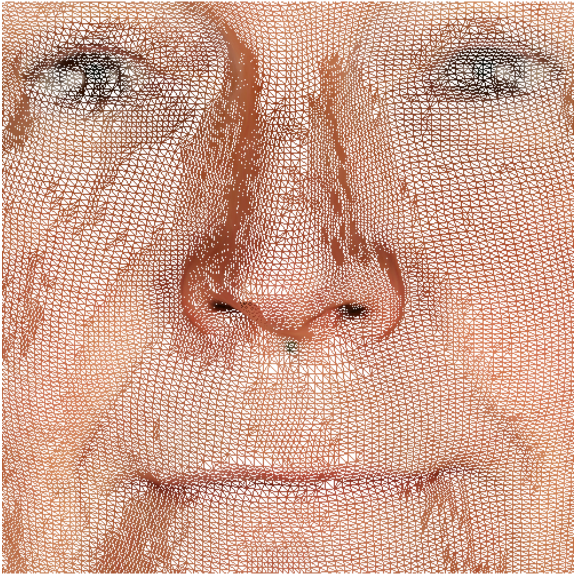

Data acquisition and pre-processing:

1. **laser-scan or stereo-camera capture**—data capture protocol (questionnaire, equipment calibration, participants, and timing)
2. **extraction of 3D coordinates, surface normals, faces (the mixture of triangles and quadrangles), and color intensity in RGB space**—from `.obj`, `.ply`, `.wrl`, and `.jpeg` files to `.dmp` files readable in R; and valid `.ply` files (with rescaled intensity) readable in Landmark software [IDAV, University of California, Davis, US]
3. **image capture validation (reliability) study**—selected distances measured with calipers, reconstruction of the coordinates, image landmarking

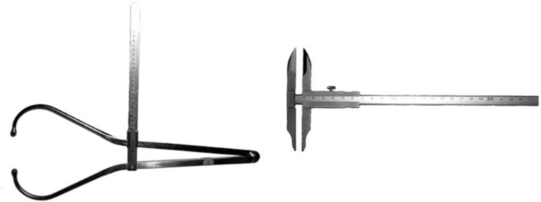

Shape Index

Smoothing vs surface inhomogeneities

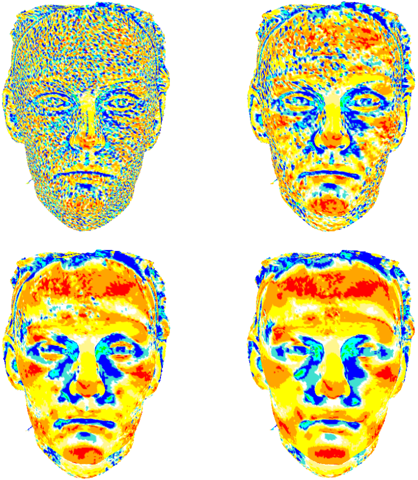

$$s = \frac{2}{\pi}\arctan\left(\frac{\kappa_2+\kappa_1}{\kappa_2-\kappa_1}\right) = \frac{2}{\pi}\arctan\left(\frac{-H}{\sqrt{H^2-K}}\right), \kappa_1 \geq \kappa_2$$

Outline:

1. the identification of anatomical curves, with the aim of providing a **much richer characterisation of surface shape than landmarks** and as a potential intermediate step to a suitable characterisation of the full anatomical surface
2. curves often define **the boundaries of particular anatomical features of interest**, allowing the position of these to be identified and, if appropriate, extracted from the larger object for separate analysis
3. types of curves:
   - **valley curve**—the curve following deepest path in the valley
   - **ridge curve**—the curve following the ridge
   - **geodesic**—shortest path between two (semi)landmarks
4. **smooth curves** across the surface with "orange peel" effect—disregarding these locally noisy areas

Surface navigation

- each anatomical surface of interest—a **two-dimensional manifold** in three-dimensional space (a suitably oriented **local surface patch**)
- while moving around this manifold it is necessary to **remain on the surface**
- a **co-ordinate system** which indexes locations on this manifold, but does not index locations off the manifold, is required
- construct local co-ordinate systems through **planar transects** of the surface, which create **one-dimensional planar curves**
- this reduces the dimensionality of the problem, while allowing the information derived from these curves to be collated across the surface at a later stage

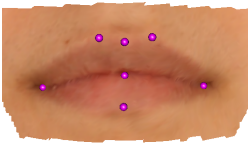

Identification of boundary points

- for each one-dimensional curve derived from the **planar transects,** the **point of intersection with the boundary curve of interest** can be identified
- these intersection points are often defined by the **locations of maximum or minimum curvature**
- on some occasions it is necessary to assess the evidence for whether any intersection point exists or whether there is more than one intersection point (points of interest)

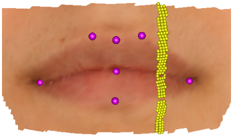

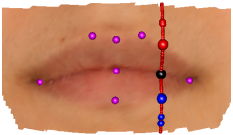

- **the collection of candidate boundary points** provides the key information from which a **boundary curve** can then be constructed

How quickly the curve bends within the surface?
geodesic curvature along a curve $\kappa(s)$ at the point $\{\widehat{x}(s), \widehat{y}(s), \widehat{z}(s)\}$ is defined as

$$\frac{\sqrt{\{\widehat{x}''(s)\widehat{y}'(s)-\widehat{y}''(s)\widehat{x}'(s)\}^2+\{\widehat{x}''(s)\widehat{z}'(s)-\widehat{z}''(s)\widehat{x}'(s)\}^2+\{\widehat{y}''(s)\widehat{z}'(s)-\widehat{z}''(s)\widehat{y}'(s)\}^2}}{(\widehat{x}'(s)^2+\widehat{y}'(s)^2+\widehat{z}'(s)^2)^{3/2}}$$

Smoothing spline idea leads to the popular **penalized least square regression** with the familiar spline penalty on the integral of the squared second derivative (Fan & Gijbels 1996)

$$\widehat{m}_\lambda(x) = \arg \min_{\forall \lambda \in \mathbb{R}^+} \sum_{j=1}^{k_c} \{x_j - m(s_j)\}^2 + \lambda \int \{m''(s)\}^2 \, dx$$

P-**spline** idea leads to the popular **penalized least square regression** with a difference penalty on coefficients of adjacent *B*-splines (Eiler & Marx 1996)

$$\widehat{m}_\lambda(x) = \arg \min_{\forall \lambda \in \mathbb{R}^+} \sum_{j=1}^{k_c} \left\{ x_j - \sum_{i=1}^{m} \alpha_i B_i(s_j) \right\}^2 + \lambda \sum_{i=d+1}^{m} (\Delta^d \alpha_i)^2$$

A **p-spline curve** takes the form of a **linear regression**, $x = B\beta$, where

- the columns of the design matrix B evaluate a set of local, **B-spline basis functions** at the values of the observed covariate
- the regression coefficients $\hat{\beta}$ minimise **the penalized sum-of-squares** $SS(\beta) = (x - B\beta)^T(x - B\beta) + \lambda\beta^T D_2^T D_2\beta$, where the matrix D_2 creates the *second differences* of the elements of the β vector

Linear constraint (Seber 1977)

- to force the solution to pass through particular landmarks
- constraint $A\beta = c$, where the columns of the matrix A evaluate the basis functions **at the constraint locations** and the vector c contains **the constrained response values**
- A has two rows which evaluate the basis functions at s_l and s_r, the arc length values at which the left and right hand corner points are located
- c is the vector (x_l, x_r)
- **the constrained coefficients** $\hat{\beta}_c$ are given by

$$\hat{\beta}_c = \hat{\beta} + (B^T B + D_2^T D_2)^{-1} A^T \left[A(B^T B + D_2^T D_2)^{-1} A^T\right]^{-1} (c - A\hat{\beta})$$

Shape constraints (Bollaerts, Eilers and van Mechelen 2006) through further use of penalty terms [in our case to adopt the anatomy of upper and lower lip to the model]

- **the penalty for monotonicity** is $\kappa\beta^T D_1^T V_1 D_1 \beta$, where the matrix D_1 constructs *the first differences* of the elements of β and the matrix V_1 is diagonal with elements which are 1 when the required monotonicity constraint is violated and 0 otherwise
- **the penalty for the second derivatives** is $\kappa\beta^T D_2^T V_2 D_2 \beta$, where the matrix V_2 is diagonal with elements which are 1 when the change in *the second differences* of the elements of β has a sign which is inconsistent with the increasing/decreasing criterion for the second derivative
- **the penalized sum-of-squares function** is now

$$SS(\beta) = (x - B\beta)^T (x - B\beta) + \lambda\beta^T D_2^T D_2 \beta + \kappa\beta^T D_1^T V_1 D_1 \beta + \kappa\beta^T D_2^T V_2 D_2 \beta$$

Symmetric Template

Symmetrically cut symmetric mesh with landmarks

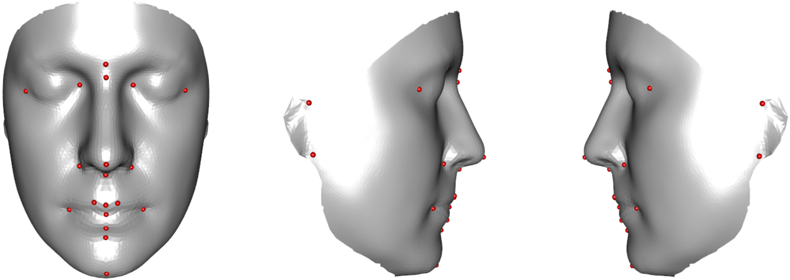

Symmetric Template

Symmetrically cut symmetric mesh with landmarks and curves

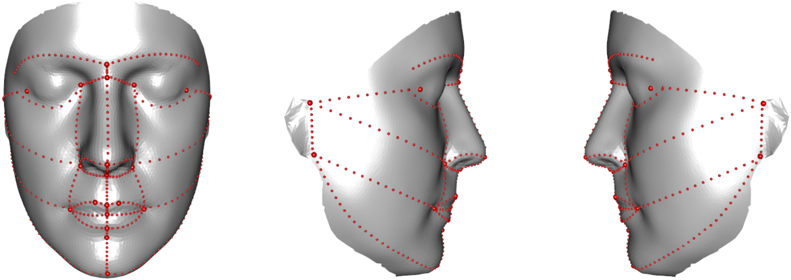

Semilandmarks on surface

Full set of anatomical curves and geodesics

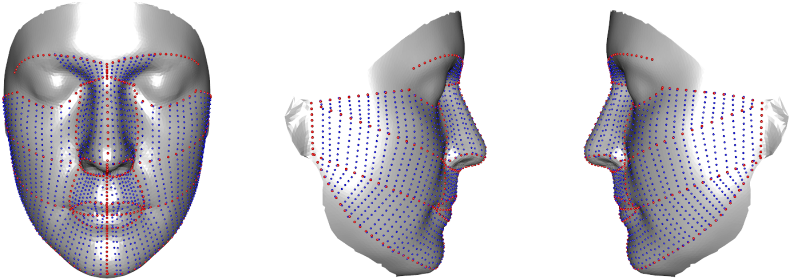

Semilandmarks on curves
Sliding – minimising bending energy

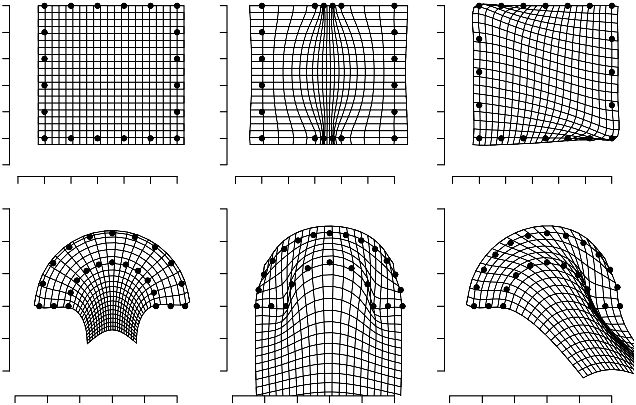

Semilandmarks on surface

Full set of anatomical curves and geodesics

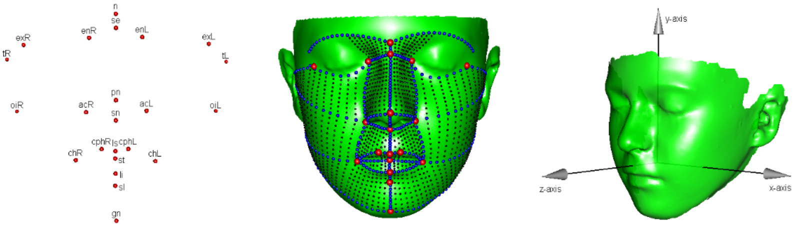
n
se
enR
enL
exR
exL
tR
tL
pn
oiR
acR
acL
oiL
sn
cphR
ls
cphL
chR
chL
st
li
sl
gn
y-axis
z-axis
x-axis

1. **landmarks**, **curves** (ridges, valleys, geodesics) [semilandmarks on curves], **surfaces** [semilandmarks on surfaces]

   the jaw line, the boundary between the lower and upper lip and surrounding skin, the philtrum valley, the nasal profile, the boundary between the nose and surrounding skin, the nasal ridge, the boundary between the lower eyelid and the surrounding skin, the brow ridges, and some geodesics on the nose and cheeks (*the areas without valleys or ridges*) between two carefully chosen anatomical landmarks
2. **automatically identified** by curvature in particular local surface patches, detection of slope discontinuities in local principal curves or optimised surface cuts
3. **a full standardised surface representation** is then available by interpolation across the relatively flat surface patches between identified curves
4. **a high resolution template** can be fitted to the semi-landmark surface by warping

3D laser-scan capture

3D facial shape–StJG data

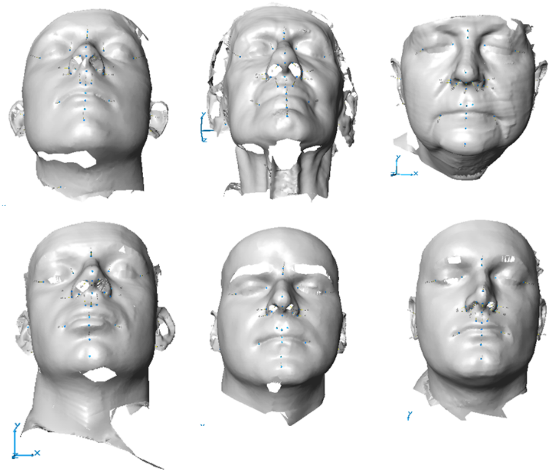

3D laser-scan capture

3D facial shape–StJG data

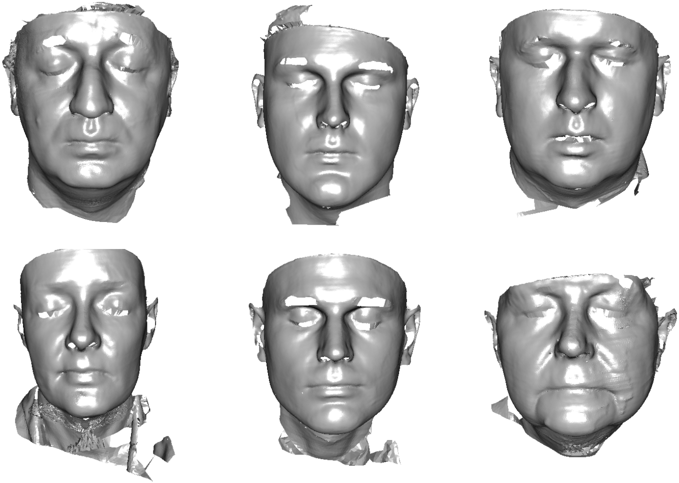

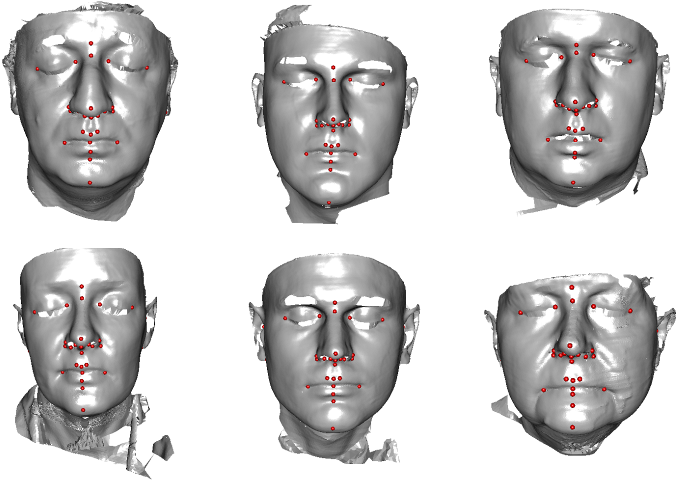

3D laser-scan capture
3D facial shape–StJG data

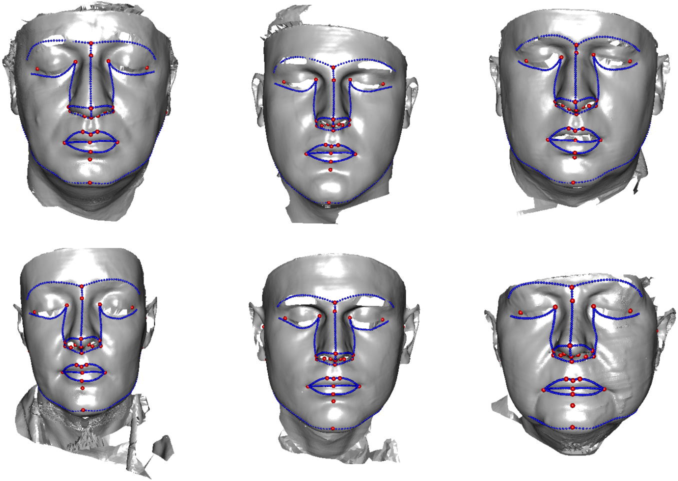

3D laser-scan capture

3D facial shape–StJG data

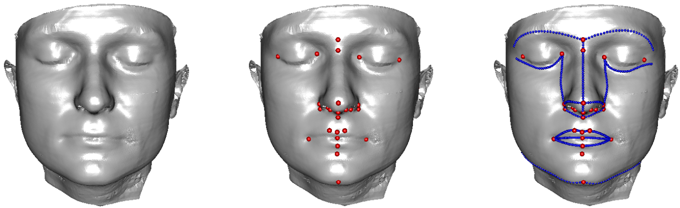

3D laser-scan capture

3D facial shape–StJG data

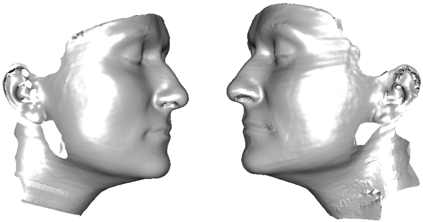

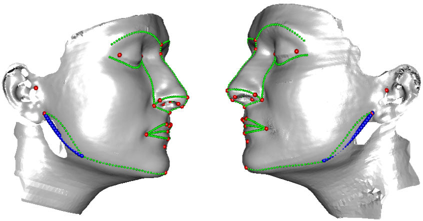

PCA for matched-pair shape data
Different types of visualisation

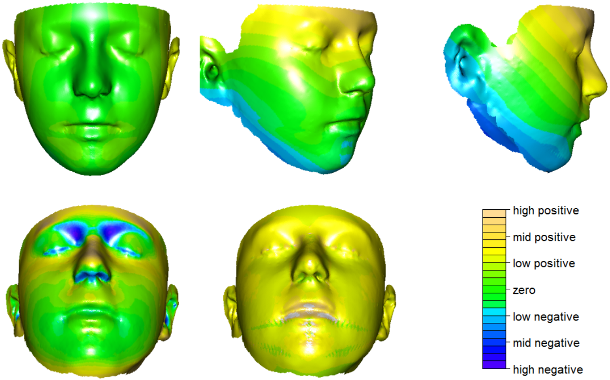

Automatic curves identification
Breast curves

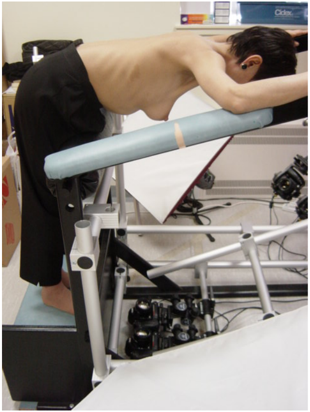

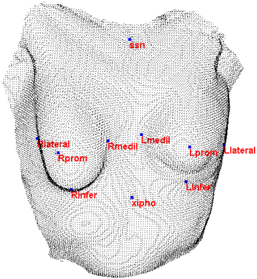

Figure: Examples of automatic breast curves identification

Automatic curves identification
Breast curves

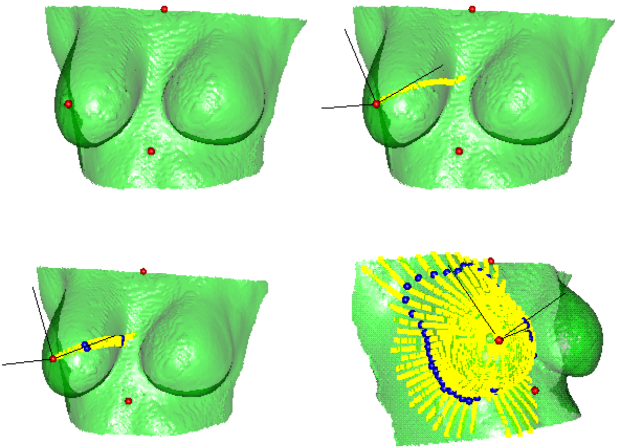

Figure: Examples of automatic breast curves identification

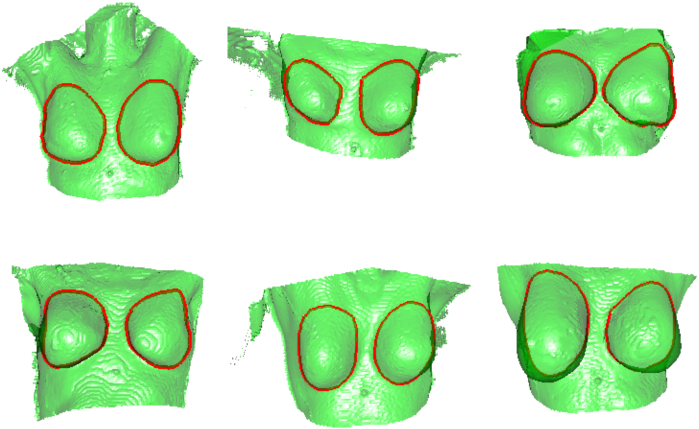

Figure: Examples of automatic breast curves identification

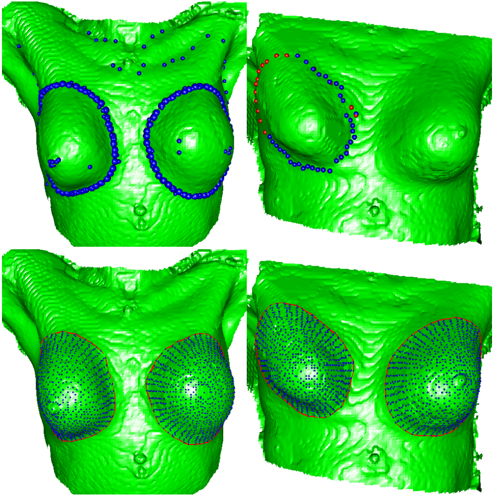

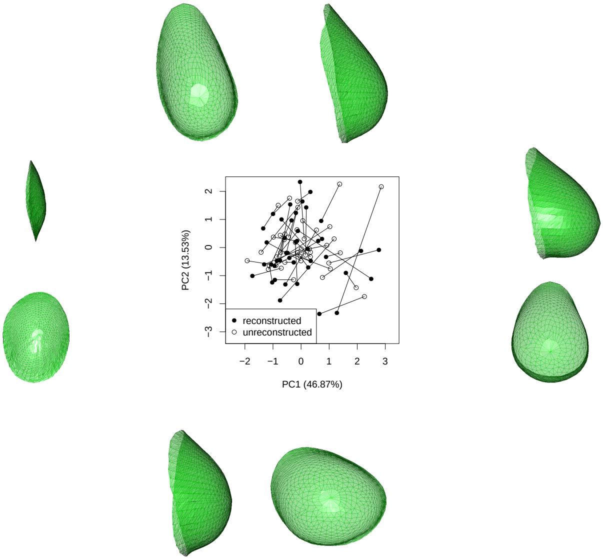

PC2 (13.53%)
PC1 (46.87%)
−2
−1
0
1
2
3
−3
● reconstructed
○ unreconstructed

Documentation for package Face3D (Version 0.1)

Tools for the analysis of three-dimensional surface images

Documentation for package 'Face3D' version 0.1

- DESCRIPTION file.

Help Pages

Face3D-package	Tools for the analysis of three-dimensional surface images
asymmetry.face3d	Construct asymmetry scores for landmark configurations
closest.face3d	Find the closest point in a face3d object
connected.face3d	Identify the connected parts of a shape object
crossproduct	Construct the crossproduct of pairs of vectors
curves.face3d	Find a planar path between anatomicaly pre-specified set of landmarks pairs through the mesh of a face3d object
display.face3d	Display the shape in an rgl window
distances.face3d	Comparing two shapes
face	A face shape
Face3D	Tools for the analysis of three-dimensional surface images
gpa.face3d	Generalized Procrustes registration of (semi)landmarks
index.face3d	Construct shape indices for a face3d object
interpolate.face3d	Thin-plate spline interpolation on the manifold, i.e. from R3 to R1
orient.face3d	Orient a face into a frontal view
planepath.face3d	Find a planar path through the mesh of a face3d object
plot.face3d	Display the shape in an rgl window
read.face3d	Read obj, pts, dilm, tps, landmarkAscii, jpg, and tif files
resamplecurves.face3d	Resample the points of a curves to pre-specified curve length
resizejpg.face3d	Resize the jpg file associated with a camera capture
rotate.face3d	Rotate the matrix of landmarks or face3d object to pre-specified planes based on carefully chosen landmarks.
rp.shapeindex	An interactive demonstration of shape indices
subset.face3d	Create a subset of a face3d object
summary.face3d	Provide a simple summary of a face3d object
warp.face3d	Thin-plate spline interpolation from R3 to R3
write.face3d	Write ply, dmp, jpg, and tif files